1996-03

Analysis of shiptrack persistence with insitu cloud measurements and satellite retrieved reflectance

Tessmer, Scott A.

Monterey, California. Naval Postgraduate School

NAVAL POSTGRADUATE SCHOOL
MONTEREY, CALIFORNIA

THESIS

ANALYSIS OF SHIPTRACK PERSISTENCE WITH INSITU CLOUD MEASUREMENTS AND SATELLITE RETRIEVED REFLECTANCE

by

Scott A. Tessmer

March, 1996

Thesis Advisor: Philip A. Durkee

Approved for public release; distribution is unlimited.

REPORT DOCUMENTATION PAGE

Form Approved OMB No. 0704-0188

1. AGENCY USE ONLY *(Leave blank)*	2. REPORT DATE	3. REPORT TYPE AND DATES COVERED
	March 1996	Master's Thesis

4. TITLE AND SUBTITLE Analysis of Shiptrack Persistence With Insitu Cloud Measurements and Satellite Retrieved Reflectance	5. FUNDING NUMBERS
6. AUTHOR(S) Scott A. Tessmer	
7. PERFORMING ORGANIZATION NAME(S) AND ADDRESS(ES) Naval Postgraduate School Monterey CA 93943-5000	8. PERFORMING ORGANIZATION REPORT NUMBER
9. SPONSORING/MONITORING AGENCY NAME(S) AND ADDRESS(ES)	10. SPONSORING/MONITORING AGENCY REPORT NUMBER

11. SUPPLEMENTARY NOTES The views expressed in this thesis are those of the author and do not reflect the official policy or position of the Department of Defense or the U.S. Government.

12a. DISTRIBUTION/AVAILABILITY STATEMENT Approved for public release; distribution is unlimited.	12b. DISTRIBUTION CODE

13. ABSTRACT *(maximum 200 words)*

Shiptracks detected on Advanced Very High Resolution Radiometer (AVHRR) satellite images posses longer detection lives and down-track brightness than expected. A simple model of physical processes is developed to correlate the ship injected aerosols to the subsequent affects on cloud condensation nuclei, droplet distribution, effective radius, and albedo. The theoretical dispersion model is tested using measured values corresponding to the terms of the model equation. The data sets consisted of insitu aircraft droplet concentration and effective radius cross-shiptrack profiles and AVHRR satellite reflectance values collected during the Monterey Area ShipTracks (MAST) experiment. Strong reinforcement of the model's droplet concentration, effective radius, and reflectance relationships is shown. The near constant value in the observed down-track fractional change of droplet concentration disputes the decreasing fractional changes of droplets predicted by dispersion associated with track widening. The results indicate down-track modification of cloud and droplet concentrations able to maintain track brightness and track detection life.

14. SUBJECT TERMS MAST, shiptrack, anthropogenic aerosol, reflectivity, correlation, remote sensing, cloud condensation nuclei, in-situ data	15. NUMBER OF PAGES 97
	16. PRICE CODE

17. SECURITY CLASSIFICATION OF REPORT	18. SECURITY CLASSIFICATION OF THIS PAGE	19. SECURITY CLASSIFICATION OF ABSTRACT	20. LIMITATION OF ABSTRACT
Unclassified	Unclassified	Unclassified	UL

NSN 7540-01-280-5500

Standard Form 298 (Rev. 2-89)
Prescribed by ANSI Std. 239-18 298-102

Approved for public release; distribution is unlimited.

ANALYSIS OF SHIPTRACK PERSISTENCE WITH INSITU CLOUD MEASUREMENTS AND SATELLITE RETRIEVED REFLECTANCE

Scott A. Tessmer
Lieutenant Commander, United States Navy
B.A., Saint Cloud StateUniversity, 1985

Submitted in partial fulfillment
of the requirements for the degree of

MASTER OF SCIENCE IN METEOROLOGY AND PHYSICAL OCEANOGRAPHY

from the

NAVAL POSTGRADUATE SCHOOL
March 1996

ABSTRACT

Shiptracks detected on Advanced Very High Resolution Radiometer (AVHRR) satellite images posses longer detection lives and down-track brightness than expected. A simple model of physical processes is developed to correlate the ship injected aerosols to the subsequent affects on cloud condensation nuclei, droplet distribution, effective radius, and albedo. The theoretical dispersion model is tested using measured values corresponding to the terms of the model equation. The data sets consisted of insitu aircraft droplet concentration and effective radius cross-shiptrack profiles and AVHRR satellite reflectance values collected during the Monterey Area ShipTracks (MAST) experiment. Strong reinforcement of the model's droplet concentration, effective radius, and reflectance relationships is shown. The near constant value in the observed down-track fractional change of droplet concentration disputes the decreasing fractional changes of droplets predicted by dispersion associated with track widening. The results indicate down-track modification of cloud and droplet concentrations able to maintain track brightness and track detection life.

TABLE OF CONTENTS

ACKNOWLEGDEMENTS

I wish to thank Professor Philip Durkee for his guidance, support, and assistance throughout my time as a student. His enthusiasm and efforts have set him apart as an instructor. His ability to give guidance only when necessary and displsy confidence enough to allow me to explore this problem my way, made the thesis process a bona fide learning experience. Additionally, thanks go to Professors Kenneth Davidson and Wendell Nuss for their moral support. Special thanks go to Commander Tom Lage for his support and labors as curriculum officer. His efforts were not unnoticed.

I owe a debt gratitude to Mr. Kurt Nielsen and Mr. Chuck Skupiewicz for their expert assistance in helping produce usable data sets. Thanks are extended to Ms. Mary Jordan for letting me employ her as a sounding board of my programming ideas.

Last but not least, I thank God for all his blessings of which my family is the most important. My success while at NPS would not have been possible without the support and encouragement of my loving, and now expectant, wife Robyn and daughter Victoria. They are my inspiration and my ground truth on which I am able to keep perspective of what is important in life. Thank you!

I. INTRODUCTION

A. HISTORY AND MOTIVATION

Since 1944 the formation and alteration of clouds has been observed over the exhaust plumes of ships. The phenomena was later described as 'anomalous cloud lines' (Conover, 1966) in visible satellite images. The satellite detected curvilinear cloud formations have been correlated to ship-generated aerosols (Radke et al, 1989) and aptly named 'shiptracks'. A natural enhancement of shiptracks in the near-infrared wavelength images (Coakley et al, 1987) has increased the observance and understanding of these cloud features. Figure 1 shows shiptracks as they appear in National Oceanic and Atmospheric Administration (NOAA) polar orbiting satellites, Advanced Very High Resolution Radiometer (AVHRR) channels one, 0.58 to 0.68μm, and three, 3.55 to 3.93μm.

The remote sensing of cloud reflectance has many significant applications. The dispersion of the pollutants (anthropogenic aerosols) and resulting modification of cloud reflectance may modify the global radiative balance and climatology. The increase in cloud albedo (reflectivity) and a corresponding decrease in the solar radiative heating response (Albrecht, 1989; Charlson et al., 1987; Charlson et al., 1992), have received considerable international scientific and media attention (IPCC, 1994) in the global warming debate. Beyond these

environmental applications, the potential use of shiptracks exists for maritime law enforcement (Rogerson, 1995) and the protection of national interests. These applications warrant the development and evaluation of aerosols reflectance modification models.

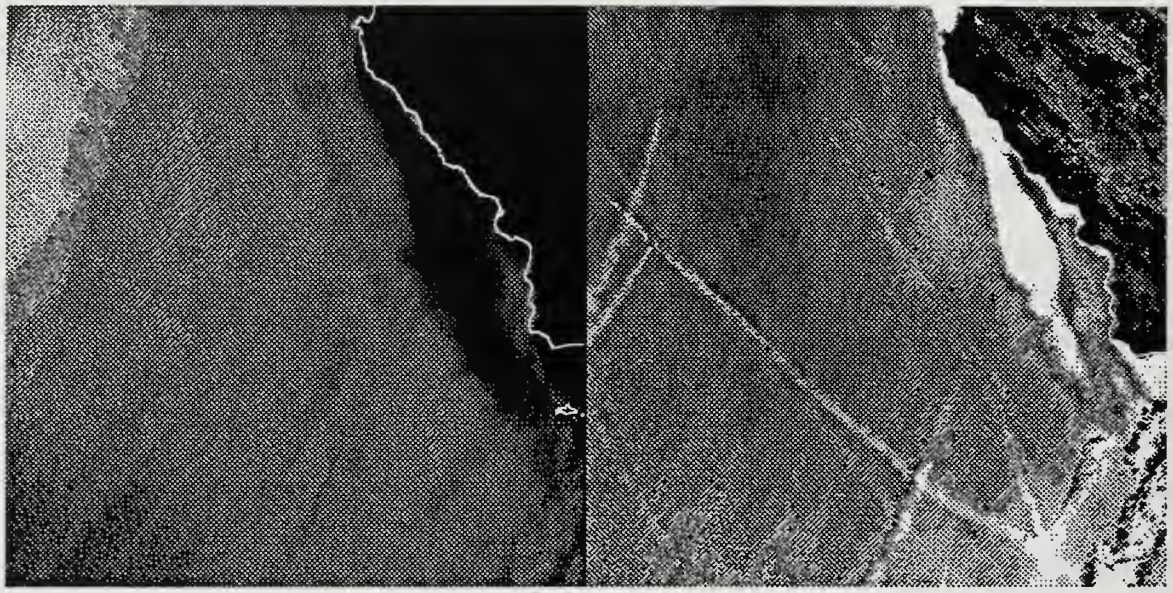

Figure 1. A comparison of AVHRR shiptrack signatures for the visible 0.63 micron wavelength (left) and near-infrared 3.7 micron wavelength (right). The image were taken on 27JUN87 2247GMT passing over the west coast of the United States. Notice the increased number and clarity of shiptracks in the 3.7 micron image.

The Monterey Area Shiptrack (MAST) Experiment (CNO Project K-1420) of June 1994 was designed to collect data for analysis of: 1)aerosol/cloud interaction and detailed microphysics; 2) boundary layer perturbation by ship; 3) cloud dynamics; and background environmental conditions, (Durkee, 1994). The eastern Pacific was chosen since it is a region known to support formation of these effects during the early summer months. The joint U.S. and United

Kingdom experiment incorporated a multi-platform data collection scheme to obtain a large and comprehensive data base on which to develop and confirm our understanding of shiptracks.

A large data base was needed to minimize inconclusive statistical variance, a trait of limited data sets, since only 27 shiptrack to ship correlations had been made prior to MAST. The MAST data set has thus far resulted in over 200 shiptrack to ship correlations (Chartier, 1995). Additionally, more than 20 aircraft missions were flown during the MAST experiment to collect critical aerosol, droplet, and gaseous information. The overall collection effort may provide the keys to understanding the shiptrack phenomena.

The atmospheric microphysical structure changes due to a ship-induced aerosol perturbation into the background airmass are detectable as an increased albedo in the near-infrared satellite image. A conceptual model, based on the hypothesis of the MAST experiment and other studies, needs to be validated. The data set of MAST permits an objective analysis of model by comparing the insitu cloud characteristics and satellite retrieved albedos. The empirical fits of the collected data will provide the model verification and direct the future analysis of ship track data to refine the model.

The fore-mentioned objective analysis and empirical fits are the tools of this thesis. However, the primary objective is the examination of a simple

dispersion model to determine the causes of a shiptrack's long life and enhanced brightness.

The remainder of this introduction provides a fundamental look at shiptrack formation and the MAST experiment climatology. Chapter II provides the theory of the shiptrack radiative enhancement by development of the physical equations from the dispersion of aerosols to the modification of the cloud reflectance. Chapter III will provide a short summary of the data sets. Methodology and analysis are addressed in Chapter IV, followed by a Chapter V comparison of the model and Aircraft to satellite results to a satellite composite analysis. Chapter VI closes with conclusions and recommendations for future analysis.

B. SHIPTRACK FUNDAMENTALS

The Advanced Very High Resolution Radiometer (AVHRR) channel three, centered at 3.7 microns, has a 1.1 km by 1.1 km resolution at nadir. The resolution and enhanced effects of CCN induced reflectance changes in the channel 3 band, make the mesoscale cloud modifications, shiptracks, discernible from the background reflectance. A variance in the background reflectance is due to the advection of continental aerosols into the Marine Atmospheric Boundary Layer (MABL) stratocumulus (Brenner, 1994). For shiptrack detection, enough CCN must be injected into the cloud to cause a resolvable change in the reflectance. The variation of background aerosol levels means a ship capable of

developing a detectable track in clean maritime air may not modify the cloud reflectance to a resolvable level in areas of strong continental advection (Brenner, 1994).

Cloud reflectance is a function of the droplet number and size distribution, liquid water content, and cloud thickness. Cloud drops are near prefect reflectors of the visible wavelengths. So for the channel one visible wavelengths, all of the described factors are of near equal importance. Therefore a change in reflectance due to a change in droplet number and size distribution appears the same as a change in thickness or liquid water content. The near infrared, AVHRR channel 3, reflectance function can be simplified due to the absorption of radiative energy. Absorption decreases the effects of liquid water content changes and cloud thickness changes on reflectance. The result for the 3.7 μm wavelength is enhanced volume scattering inversely proportional to the particle radius, i.e.; backscattering effectiveness increases with smaller radii. Furthermore, absorption effects cause clouds of 100 meters or greater thickness to be equally efficient scatterers. These phenomena simplify the near infrared reflectance dependence to be inversely proportional to the water droplet effective radius for stratiform clouds thicker than 100 meters.

Changes in droplet radius are induced by the addition of CCN by ships. The additional aerosols, as depicted in Figure 2, compete for moisture, increasing the droplet concentrations and decreasing the clouds' effective

droplet size. Aircraft measurements taken in the relative wind 'wakes' of ships; at levels below, in, and above the cloud layer; confirm that modifications have been made by the ships (King, et. al. 1993).

Ships create sea surface wakes which introduce sea salts into the atmosphere, cause turbulent atmospheric wakes which induce mixing in the boundary layer, and produce heat, gases, and particles in their exhaust which provide CCN and mixing(Hindman, 1990; Porch, et al., 1990). The complexity of shiptracks is illustrated by the aforementioned direct mechanisms and the later effects of gas to particle conversion and possible instabilities due to differential heating (cooling) of the background by the modified cloud. Figure 2 also shows that a temporal and spatial offset exists from the ship to the 'track head', the nearest point of detectable cloud modification and usually the most intense area of cloud reflectance contrast.

A comprehensive collection of shiptrack to ship correlations have been made and analyzed for their overall characteristics (Chartier, 1995) and the average ship to track-head offset (Rogerson, 1995). Chartier described the typical shiptrack as being detectable for hundreds of kilometers and one to two days, and yet having a width of only 8-12 kilometers. An apparent resistance to dispersion, cloud condensation nuclei production, or other mechanisms might explain these attributes. The theoretical examination and data analysis of aerosol dispersion, condensation nuclei concentration, effective radius, and

reflectance in the following chapters attempts to clarify the influences affecting shiptrack characteristics.

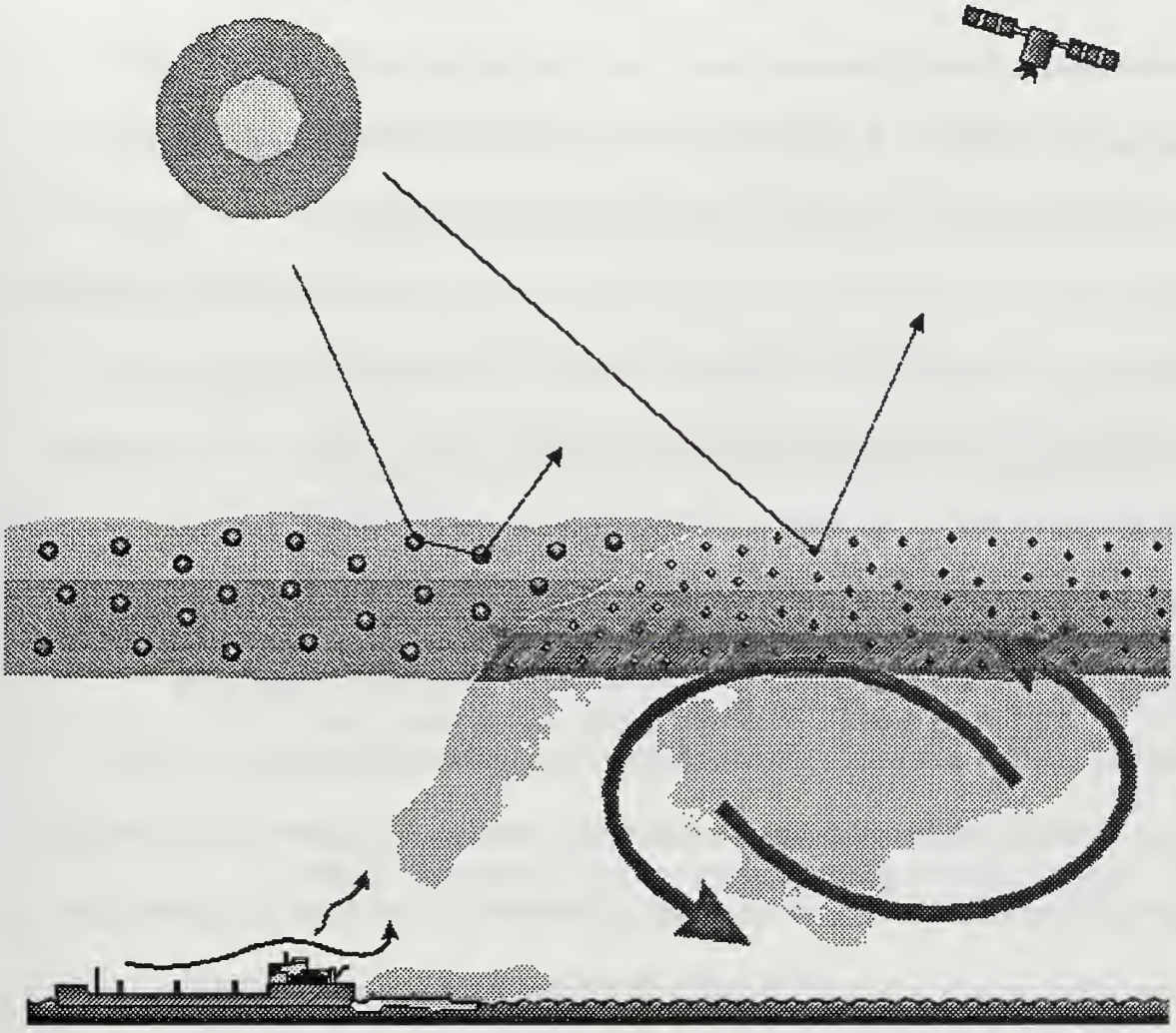

Figure 2 The formation of shiptracks in the Marine Atmospheric Boundary Layer. The cloud layer is represented by the shaded layer with droplet sizes and numbers represented within the layer. The thin lines represent the 3.7 μm solar radiation and the modified scattering. Turbulent mixing is indicated by the large arrows, while the thin curved lines represent buoyancy due to exhaust heat and mechanical turbulence produced by the ships motion. From Brown (1995).

C. BACKGROUND ENVIRONMENTAL CONDITIONS

Under the influence of seasonally persistent high pressure, the eastern ocean basins, west continental coasts, provide the necessary conditions for shiptrack formation. A shallow, cloud topped, and well mixed boundary layer combined with a low number of CCN, and a narrow range of temperature and humidity are regarded as the necessary conditions for shiptrack formation (Conover, 1966; Trehubenko, 1994). The eastern Pacific is typically dominated by a subtropical high induced by the Hadley Cell circulation during the month of June. The presence of this high produces a strong capping substance region with extensive stratiform clouds. The northerly currents in the Pacific below the air mass provide a moist and cool surface to assist the development of a strong, shallow Marine Atmospheric Boundary Layer. For June 1994, the time of the MAST experiment, the hope to exploit this climatology met with limited success. While a vast data base was collected, the potential for more shiptracks was lost to unusually fair conditions for a portion of the experiment. A complete daily synoptic summary is an appendix in Brenner, 1994.

II. THEORY

A. THE MAST HYPOTHESIS

The MAST experiment proposed several hypotheses to be tested. The working hypothesis is summarized below (Durkee, 1994), not all issues will be addressed in this comparison.

1 Aerosol/cloud interactions and detailed microphysics

- 1.1 Submicron aerosols from ship's exhaust and water wake are responsible for the cloud droplet and radiative features of shiptracks
- 1.2 Precipitation is reduced and column liquid water content increased by the stabilization of the drop size distribution from the aerosol, CCN, injection.
- 1.3 Gas to particle conversion provides a down track CCN source for cloud modification.
- 1.4 Ship enhanced entrainment of aerosols from above the MABL increases drop formation reducing droplet size and increases cloud albedo.

2 Boundary Layer Perturbations by the Ships.

- 2.1 Shiptracks enhance buoyancy and vertical motion affecting cloud formation by moisture and heat injection.
- 2.2 Mechanically generated turbulence and perturbations modify the MABL and assist in the formation of cloud features.

3 Cloud Dynamics

- 3.1 Cloud reflectance and LWC changes cause a radiation induced circulation that stabilize and confine the shiptrack.

3.2 The track maintains its form due to enhanced vertical motion within the track from the release of latent heat by condensation.

4 Background Environmental Conditions

4.1 A shallow MABL depth and low CCN concentration combined with preexisting cloud formation mechanisms are required to form shiptracks.

4.2 Shiptracks are reduced by a decoupled MABL by limiting the mixing of ship induced aerosols to the upper MABL cloud layer.

The premises listed above are a starting point for the modeling of reflectance from droplet size. Simplifications during specific stages of analysis are required to yield a functional model. For the model used in this investigation, an overall assumption of no precipitation within the shiptrack has been implemented to conserve liquid water mass concentration (MAST working hypothesis 1.2).

B. THE PROPORTIONALITY OF TRACK WIDTH TO PEAK REFLECTANCE AT 3.7 MICRONS

The sensitivity of cloud albedo to changes in the CCN concentration is referred to as cloud susceptibility (Platnick et al, 1994). In the case of shiptracks, it is reasonable to go one step further and start with the relationship of shiptrack width to the CCN concentration. The fractional change of a quantity will be normalized to the mean value across the change, $\partial X / \overline{X}$ for a given parameter X. Equation one characterizes the physical processes from a dispersive fractional change in track width to a detected fractional change in track reflectance. The

variables are as follows: shiptrack width (σ); cloud condensation nuclei as a concentration (CCN); activated droplet number (N_d); effective radius (r_{eff}); and reflectance at the 3.7μm wavelength (ρ (3.7)).

$$\frac{\partial \sigma}{\sigma} \Rightarrow \frac{-\partial\, CCN}{CCN} \Rightarrow \frac{-\partial N_d}{N_d} \Rightarrow \frac{\partial r_{eff}}{r_{eff}} \Rightarrow \frac{-\partial \rho_{(3.7)})}{\rho_{(3.7)}} \qquad 1$$

The normalized fractional change in track width to the fractional change in cloud condensation nuclei interdependence,

$$\frac{\partial \sigma}{\sigma} \propto \frac{-\partial\, CCN}{CCN}, \qquad 2$$

is a simplified representation of a dispersion only process. The track width can be reduced to a one dimensional cross section defined by the time of aerosol emission and relative wind, assuming that the cloud thickness is constant in depth over the area. While this assumption does introduce error, it is a favorable starting point in building a verifiable model.

The right side, fractional change in cloud condensation nuclei, is represented as a directly inverse relation based on one dimensional dispersion, provided there are no changes in the overall concentration. Gas to particle conversion (MAST working hypothesis 1.3) or aerosol modification by condensation and evaporation processes are two plausible condensation nuclei concentration-modifying processes able to induce error. Here, the information derived from an empirical fit of the data will advance the understanding of the fractional change in CCN. The empirical fit value will include the dispersion

effects and any additional time dependent processes, such as gas to particle conversion, dry deposition to the sea surface, wet deposition via precipitation, and aerosol-modifying cloud processes.

The next relationship to be examined is the fractional change in CCN to the fractional change in droplet number. The relationship of the change in CCN to droplet number has been evaluated experimentally to be approximately linear (Platnick et al, 1994). The background environmental conditions to form shiptracks require that there is an initial low number of CCN. Additionally, the injected aerosol must be hydroscopic and able to scavenge liquid water by having a lower equilibrium saturation than the initial cloud. With the second background condition of well mixed MABL, the aerosol distribution can be considered homogeneous within a MABL column and only changing with the width of the track itself. Normalization of the change in CCN and change in droplet size will not effect the linear relationship. Under these conditions this relationship can be expressed as being approximately linear,

$$\frac{\partial CCN}{CCN} \propto \frac{\partial N_d}{N_d}. \qquad 3$$

The preservation of the droplet distribution shape is important in relating the fractional change in droplet number to the fractional change in effective radius. Under the previously stipulated assumption of no precipitation, there is conserved liquid water content ,LWC, in the cloud column. The observed value in a typical marine atmospheric boundary layer is approximately $0.3 g/m^3$

independent of the amount of CCN present (Noonkester, 1984). Holding the LWC constant conserves the total volume in a homogenous, constant water density, MABL. The correlation between the parameters is derived using the volume formula;

$$V = \frac{4}{3}\,\pi\, N_d\, r_n^3\, F(3), \tag{4}$$

where

$$F(3) = \frac{\Gamma(\alpha + 3)}{\Gamma(\alpha)}, \tag{5}$$

and $\Gamma(\alpha)$ is a gamma function distribution (Stephens, 1994). Using a derivative of the volume with respect to time and the chain rule

$$\frac{dV}{dt} = \frac{\partial V}{\partial N_d}\frac{\partial N_d}{\partial t} + \frac{\partial V}{\partial r_{eff}}\frac{\partial r_{eff}}{\partial t} = \text{constant}, \tag{6}$$

the conservation of volume results in the relationship

$$\frac{\partial N_d}{N_d} = -3\frac{\partial r_{eff}}{r_{eff}}. \tag{7}$$

Lastly, the fractional change in effective radius to the fractional change in the 3.7 micron reflectance (albedo) can be established. Mineart (1988) modeled the marine stratiform clouds using a gamma distribution with modal radii of four and 8 microns, typical of marine air mass. Siquig (1991) continued this investigation following the same assumptions as Mineart. Both examinations correlate the reflectance to approximately the inverse of the modal radius . The

use of the effective radius in this model vice the modal radius (r_d) is resolved by the relationship

$$r_{eff} = \frac{(\alpha+3)}{(\alpha-1)} r_d, \quad 8$$

which normalizes to the linear relationship

$$\frac{\partial r_{eff}}{r_{eff}} = \frac{\partial r_d}{r_d}, \quad 9$$

allowing the use of the fraction change in effective or modal radius (Stephens, 1994).

The approximation of the Mineart and Squig relationships,

$$\rho_{(3.7)} \cong A / r_d, \quad 10$$

and Equation 9 yield the final relationship

$$\frac{\partial r_{eff}}{r_{eff}} = \frac{-\partial \rho_{(3.7)}}{\rho_{(3.7)}}. \quad 11$$

The proportionality relationships resolved in Equations 2, 3, 7, and 11 give the overall theoretical relationship,

$$\frac{\partial \sigma_y}{\sigma_y} = \frac{-\partial\, CCN}{CCN} = \frac{-\partial N_d}{N_d} = 3\frac{\partial r_{eff}}{r_{eff}} = -3\frac{\partial \rho_{(3.7)}}{\rho_{(3.7)}}. \quad 12$$

The next step to validate the formulated dispersion only model (Equation 12) is to designate and analyze data sets for each individual relationships between the fractional change in track width and the fractional change in reflectance.

III. DATA SETS

A. AIRCRAFT DATA SET

A United Kingdom C-130 Hercules airplane was one of several airborne platforms performing data collection in association with the Monterey Area ShipTracks (MAST) experiment. Other airborne platforms included a University of Washington C-131, a NASA ER-2, and the US/LTA 138S Airship. The Meteorological Research Flight facility of Farnbough, UK conducted the scientific measurements and flight operations. The aircraft has a flight radius of 5,550 km and an endurance of 11 hours.

A temporary operations center at the Naval Postgraduate School in Monterey, CA directed flights during the test, dispatching the aircraft to satellite detected shiptracks. During the month long experiment, the C-130 flew eleven data collection flights investigating twenty ships. The aircraft was not always able to find the satellite shiptrack or was prevented by flight restrictions to fly through the track while in the cloud. This greatly limited the number of in-cloud cross track flight profiles available to 28. Cases examined are restricted to in-cloud flights since the entrainment induced variability near cloud edges could bias the data with lower liquid water contents. The theoretical assumption is that liquid water mass is conserved. Complete flight equipment status, flight profiles, and general narrative summaries are available in the MAST Flight

Summary for the U.K. C-130 (Gibbs, et al., 1994). A summary of the flight data used in this analysis is given in Table 1.

Flight number	GMT date	Julian day	Ships of interest	In-cloud track crossings
A334	08 June	159	Keystone Canyon	1
A335	09 June	160	Newport Bridge	4
A338	13 June	164	USS Safeguard Sanko Peace	8 3
A346	27 June	178	Cosco Tai He	6
A347	28 June	179	Evergreen Ever Genius	3
A348	29 June	180	Hanjin Barcelona	3

Table 1 A summary of C-130 flights with mid cloud shiptrack passes (after Gibbs, et al., 1994).

The aircraft recorded standard meteorological and flight parameters in addition to the following sensor's measurements:

1) passive cavity aerosol spectrometer probe, PCASP, for 0.1 to 3.0μm diameter aerosols;

2) forward scattering spectrometer probe, FSSP, for 0.5 to 47μm diameter aerosols and droplets;

3) two dimensional optical array probes for 25 to 800μm diameter droplets and 200 to 6400μm diameter precipitation drops;

4) thermal gradient diffusion chamber for the chemically defined cloud condensation nuclei spectra;

5) and Pollak counter for total condensation nuclei values.

The forward scattering spectrometer probe (FSSP) measurements, standard meteorology parameters, and flight parameters are used in this analysis. This is dictated by the size spectra for the cloud concentration nuclei, CCN, and cloud droplets in non-precipitating marine stratus.

The FSSP collected data, listed above, has bulk parameter values at one second intervals. A complete description of the aircraft data sets, calibrations, and post flight processing is giving in A guide to the Data from the Meteorological Research Flight held within the M.A.S.T. data archive (Percival, 1995). The processed data of the FSSP is provided in a matrix format with quality control flags associated with less than nominal quality data values. Before further processing any data in association with this study, all flagged data points were replaced with a non-numeric value. The FSSP measurements correlated in this hypothesis test are the bulk concentration, cm^{-3}; liquid water content, g/kg; and effective radius, μm.

Aircraft corrected position and winds are further entries. The corrected values are composites of the inertial navigation system, global positioning system, omega navigation system, and wind vanes measurements. The final values are composed of the northward and eastward wind speeds and decimal degrees of latitude and longitude averaged over each second of flight. The data analysis of the cross track collection runs permit the use of a beta-plane assumption and the use of a Cartesian coordinate system. Chapter IV will detail the data interpretation scheme for the individual flight and sensor parameters.

B. SATELLITE DATA SET

The prime detector of shiptracks are the AVHRR satellite sensors. The Naval Postgraduate School (NPS), Remote Sensing Laboratory, within the Meteorology Department, collects and archives polar orbiting satellite images. The MAST satellite data set was collected and processed at the NPS Remote Sensing Laboratory and has been analyzed in several other thesis's including the references Brenner (1994), Brown (1994), Chartier (1995), Rogerson (1995), and Trehubenko (1994). The following paragraphs will summarize the collection and processing of the shiptracks.

During the MAST experiment, up to ten passes per day of NOAA 9/10/11/12 AVHRR polar orbiting satellites images of the eastern North Pacific were collected. The largest gap between passes was six hours; however, night time passes are not applicable to this study. The images yielded 1362 track heads and 735 shiptrack extraction using a algorithm developed by Nielsen and Durkee (1992). The head positions and tracks were correlated by Brown (1995) and Chartier (1995) to actual ships using several sources. For this application, only correlated shiptracks with aircraft in-cloud cross track runs are usable. The Cosco Tai He, flight A346, and the Hanjin Barcelona, flight A348, were the only two cases where both satellite correlated imagery and aircraft runs occurred within six hours of each other providing an initial set of nine cross track runs to compare to satellite imagery.

Processed NOAA channel 3 imagery is utilized in this study. The clouds that are not low stratiform, stratocumulus, are removed using an algorithm with inputs from channels 1 through 5 (Skupniewicz, 1995). Then a correction factor to remove brightness bias due to anisotropic reflectance was applied. This equalized the pixel brightness due to sun and satellite angle differences across the images and between different passes. The result is an absolute reflectance image of low clouds centered in the 3.7μm band, channel 3, referred to as LOW3 in previous NPS thesis's.

At this point, shiptrack extraction's using the Nielsen and Durkee (1992) algorithm was applied. The shiptrack is transformed to a matrix of brightness values centered on the brightest pixel, 1km by 1km, and 61 pixel wide, perpendicular to the shiptrack. The length of the matrix is the total track length to a maximum of 1000km, pixels. Since the tracks are not straight lines, they are divided into line segments of different orientations to approximate the curvature. The segments are defined by the latitudes and longitudes of their end points. The resulting data can then be translated with the ship's course and speed and compared to aircraft data. The following chapter on methodology and analysis details the process of integrating these two data sets.

IV. METHODOLOGY AND ANALYSIS OF RELATIONSHIPS

A. THE FRACTIONAL CHANGE OF EFFECTIVE RADIUS VS THE FRACTIONAL CHANGE OF DROPLET NUMBER

The relationship between the fractional change of effective radius and the fractional change of droplet number is the chosen starting point in the analysis of the theoretical relationship between track width and track reflectance. Since both data sets are collected by the same source, the MRF C-130, no corrections for temporal or spatial offset need be considered. An initial analysis of the FSSP data set of drop concentration, effective radius, and liquid water content was used to test the MAST assumptions and theoretical relationship presented in Equation 7. The aircraft FSSP measurements provide the data to fit the relationship of the fractional change of effective radius to the fractional change of droplet number. An additional benefit is the increased statistical significance provided by the larger size of the data set.

The FSSP measures the concentration of droplets between 0.05 and 47 μm in diameter. In a cloud at equilibrium saturation and with the conservation of liquid water mass, Equation 7 yields the algebraic relationship

$$\frac{\Delta\ (\text{FSSP concentration})}{\text{FSSP concentration}} = C\frac{\Delta r_{eff}}{r_{eff}}, \qquad 13$$

where C, a linear regression value, should theoretically be negative three.

The right-hand side of Equation 13, fractional change in effective radius, is a post flight processed quantity of the FSSP measurements and was calculated by the Meteorological Research Flight (Percival, 1995). Table 1 lists the flights comprised in the data set for this relationship. Each one second interval measurement from the in-cloud cross-track runs is a data point. The unedited data, 10,399 points, was analyzed to find the linear regression value, *C*, from Equation 14, independent of liquid water content. In initial observations, it was immediately apparent that the LWC was not consistent across track or down track. Data comparisons of the fractional change of concentration to the fractional change of effective radius yielded the distribution shown in Figure 3.

The distribution, independent of constraints, shows noise that may be skewing the regression. A refined approach was to analyze the data regression values and interactions as LWC levels changed. The LWC dependent values revealed three distinct regions across the LWC values, Figure 4. The initial region, up to 0.05 g/m^3 LWC is described by a decreasing value in the concentration to effective radius fractional change regression. The non-constant regression values may be an indication of the cloud formation and scavenging process while not yet at saturation equilibrium. The formation and scavenging period would be characterized by pockets of moist air and dry air interspersed and causing a wide range of growth and decay rates with saturation levels. The scavenging process is also the reason for excluding aircraft runs either at the top

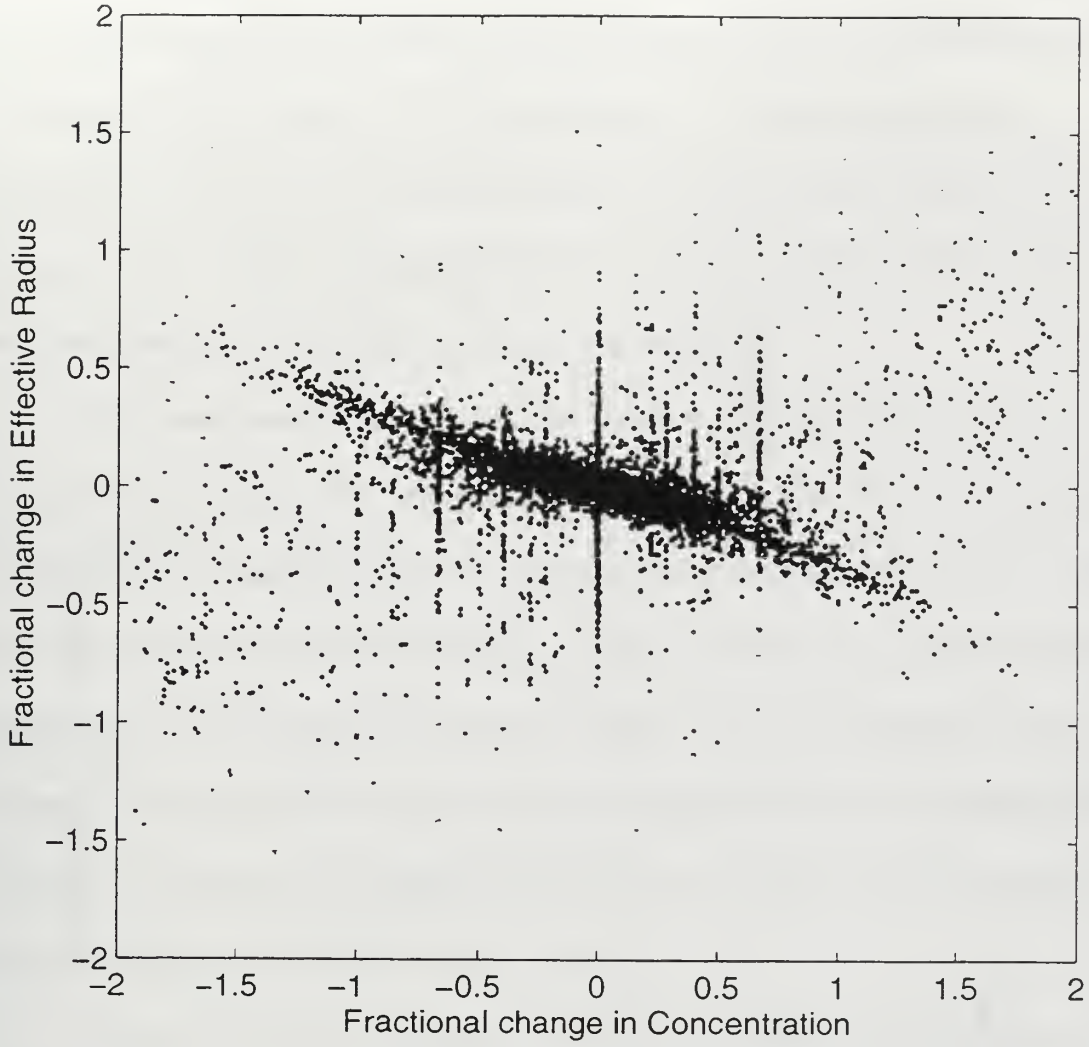

Figure 3 The fractional change of concentration to the fractional change of effective radius for all data points independent of LWC.

or base of the clouds, minimizing the effects of entrainment fluctuations. The non-constant nature of this low LWC region precludes its use, independent of the specific causes which are beyond the scope of this study.

The other area of decreasing regression values, greater than 20 g/m^3, will also be excluded from this study. Again, the regression values are not constant with

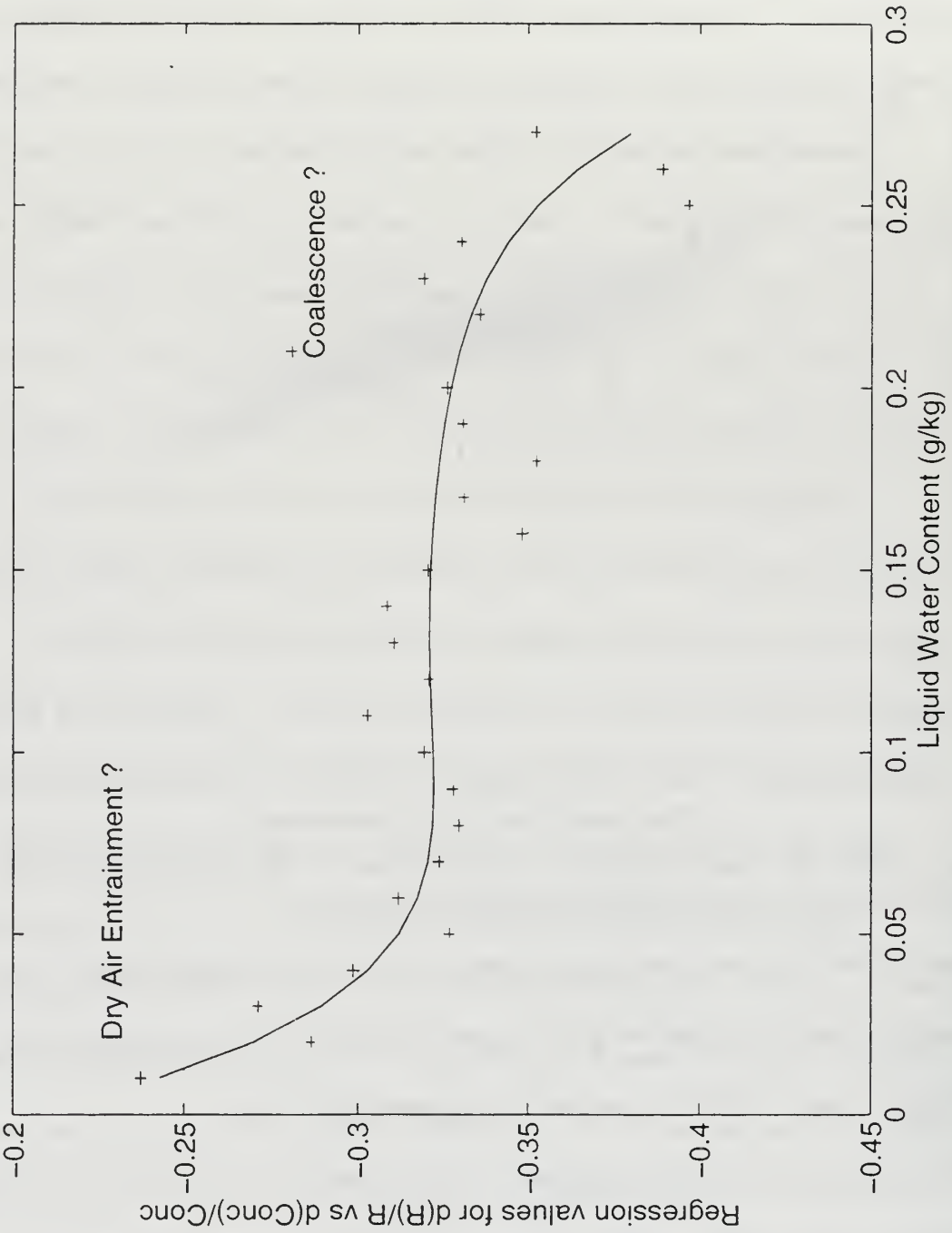

Figure 4 The fractional change of concentration to fractional change of effective radius regression values verse LWC.

LWC, indicating that processes other than dispersion may be contributing to the change in effective radius. A likely explanation causing the decreasing regression values would be the beginning of the collision and coalescence process which would rapidly modify droplet size and number distribution without changing the effective radius for a given LWC.

The requirements for a cloud to be stable, comprised of droplets at saturation equilibrium and non-precipitating, limit the data set to cases where effective radius changes only as a function of the change in concentration. The LWC limitations from 0.05 to 0.20 g/kg constrain the data set to 6628 fractional change pairs, where pairs are exclusively within a track. To minimize over-representing individual tracks, pairs are formed only with the neighboring valid points. This means three points yield two pairs as opposed to the three pairs possible if all combinations are considered.

Figure 5 shows the regression analysis of the stable cloud data set and significant reduction in noise from the LWC independent case. This stable case produces a clearly defined correlation between the fractional change of effective radius and the fractional change of droplet number. A regression value of -0.32248, with a standard deviation of 0.03188, approximately 10%, was calculated for the stable sub-set data. This value, represented by 1/c in Equation 13, yields the relationship

$$\frac{\Delta\,(\text{FSSP concentration})}{\text{FSSP concentration}} = \frac{1}{0.03188}\,\frac{\Delta r_{eff}}{r_{eff}} = -3.1011\,\frac{\Delta r_{eff}}{r_{eff}}, \qquad 14$$

which will be substituted in to Equations 7 and 12. This value and it's associated standard deviation agree extremely well with the theoretical value.

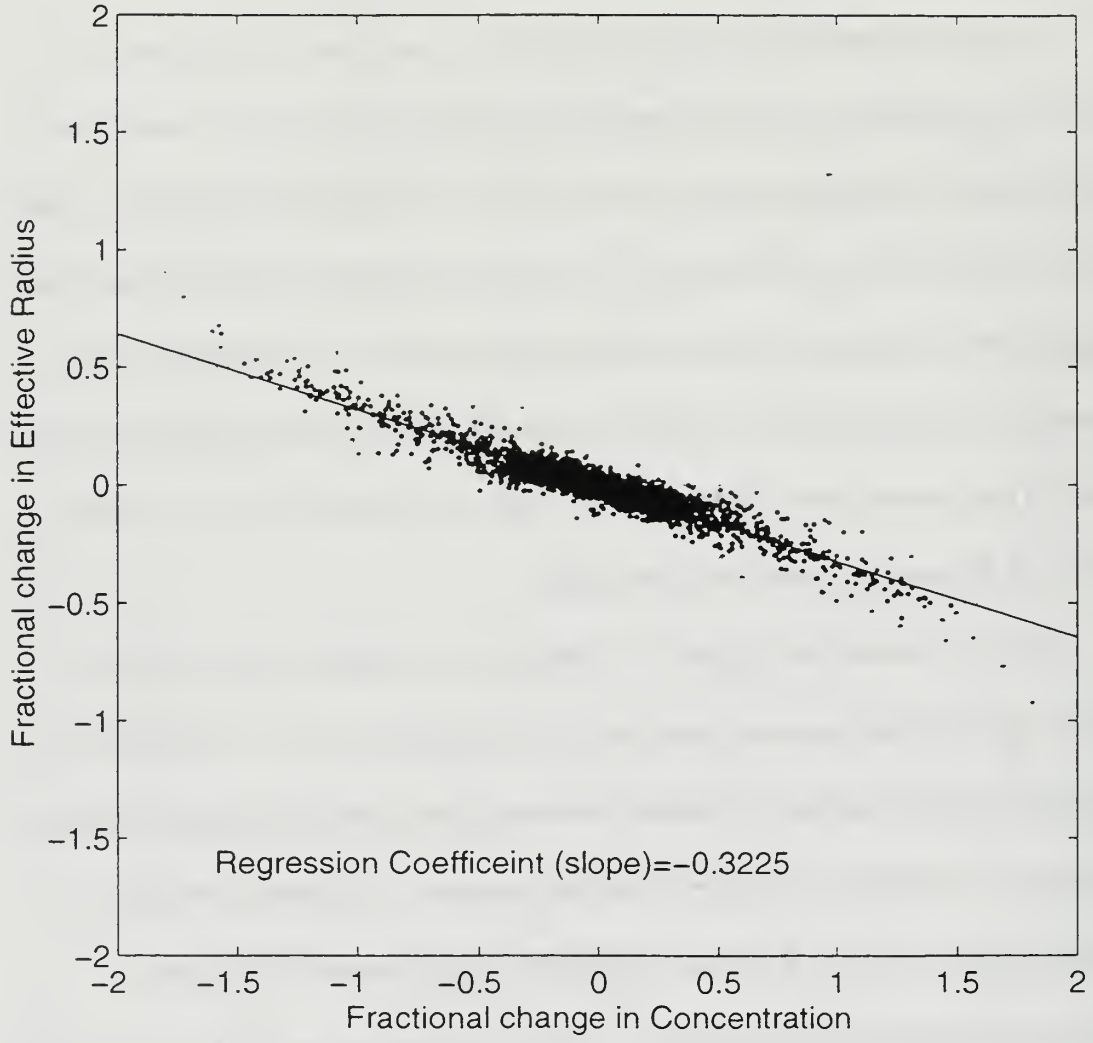

Figure 5 The fractional change of concentration to fractional change of effective radius regression values verse LWC of the stable cloud data set.

B. THE FRACTIONAL CHANGE OF SATELLITE REFLECTANCE VS THE FRACTIONAL CHANGE OF EFFECTIVE RADIUS

A comparison of the fractional change of satellite reflectance to the fractional change of effective radius is the second relationship in the testing of the theoretical equation of the fractional change in track width to the fractional change in peak track reflectance, Equation 12. The data sets in this case are very limited, since there must be a correlated shiptrack image that the aircraft data can be compared against. In defining this set, several assumptions must be made and conditions set to meet the assumptions.

The assumptions required are that the track shape and along track relative reflectance are preserved. This implies that the track physics of turbulence and dispersion do not change significantly and that meteorological conditions are persistent and stable. These situations are most probable over short time periods. In finding cases that best fit the condition, the data set narrowed further. Sortie A346 on the Cosco Tai He, Table 2, and sortie A348 on the Hanjin Barcelona, Table 3, had correlated satellite images within six hours of the flights. These two data sets contain nine aircraft data runs through cloud.

The methodology of matching satellite reflectance data to the aircraft runs is described in next few paragraphs. The first step is the quality control of the aircraft data to remove all data points where the liquid water content is not in

Run	Historical position. (GMT)	Run start time (GMT)	Run end time (GMT)	Aircraft altitude (feet)	Ship's true heading and speed (knots)
1	17:54:07	18:05:40	18:10:11	1500	120° @ 17.5
2	17:54:07	18:14:52	18:20:41	1500	120° @ 17.5
3	17:54:07	18:22:42	18:28:00	1500	120° @ 17.5
4	20:00:00*	21:20:13	21:28:50	1500	135° @ 17.5
5	20:00:00*	22:13:47	22:19:36	1300	135° @ 17.5
6	20:00:00*	22:43:08	22:47:39	1400	135° @ 17.5

Table 2 A summary of correlated cross track, in-cloud aircraft runs commencement times for the Cosco Tai He on 27 June, 1994, flight A346 (Gibbs, et al, 1994). Reflectance images where from the NOAA 9 polar orbiting satellite at 1753 GMT of 27 June, 1994. * Runs 4, 5, and 6 historical position is from a dead reckoned heading change position.

Run	Historical position. (GMT)	Run start time (GMT)	Run end time (GMT)	Aircraft altitude (feet)	Ship's true heading and speed (knots)
1	18:17:45	18:43:00	18:46:39	2000	118° @ 23.1
2	18:17:45	19:13:30	19:16:22	2500	118° @ 23.1
3	18:17:45	20:31:18	20:43:49	2200	118° @ 23.1

Table 3 A summary of correlated cross track, in-cloud aircraft runs commencement times for the Hanjin Barcelona on 29 June, 1994, flight A348 (Gibbs, et al, 1994). Reflectance images where from the NOAA 9 polar orbiting satellite at 1727 GMT of 29 June, 1994

the range specified in the initial relationship comparing fractional changes in effective radius and concentration (see section A of this chapter). The limits of liquid water content, between 0.05 and 0.20 g/m^3, are applied to maintain consistency within the overall relationship described in Equation 12. When a specific example will aid in clarification of a process, the case of the Cosco Tai He cross track run number six of 27 June will be used since it represents the

extreme for nearly all corrections. All runs have been corrected by the same means described in these examples.

The satellite data is set up in a matrix of cross track pixels and down track distance. The center bins are defined along a line with geographical matched endpoints. The geographic positions embedded in the track allow the translation of the reflectance data to match the current ship position. Figures 6 shows the original track and the translated track for the Cosco Tai He run six. The historical ship's position at the time of the image is defined by the track head position from the image and the mean track offset, 4.6 NM for the Tai He, as derived by Rogerson (1995). This historical position and the aircraft's ship mark on top positions are used to determine the direction and distance of the translation. The satellite image closest to the aircraft run time is utilized which in all cases was of equal or better quality than other images that day and was nearest to local apparent noon, reducing shadows and anisotropic reflectance corrections.

The ship position and translated track are geographically corrected to the proper location for a specific cross track run center time. The center time of the run is determined using a 21 second average maximum, approximately 2 km for typical aircraft speeds, of FSSP measured particle concentration for the specific run. Figure 7 illustrates the corrected positions for the Cosco Tai He cross track run number 6. These preliminary corrections do not precisely correlate the

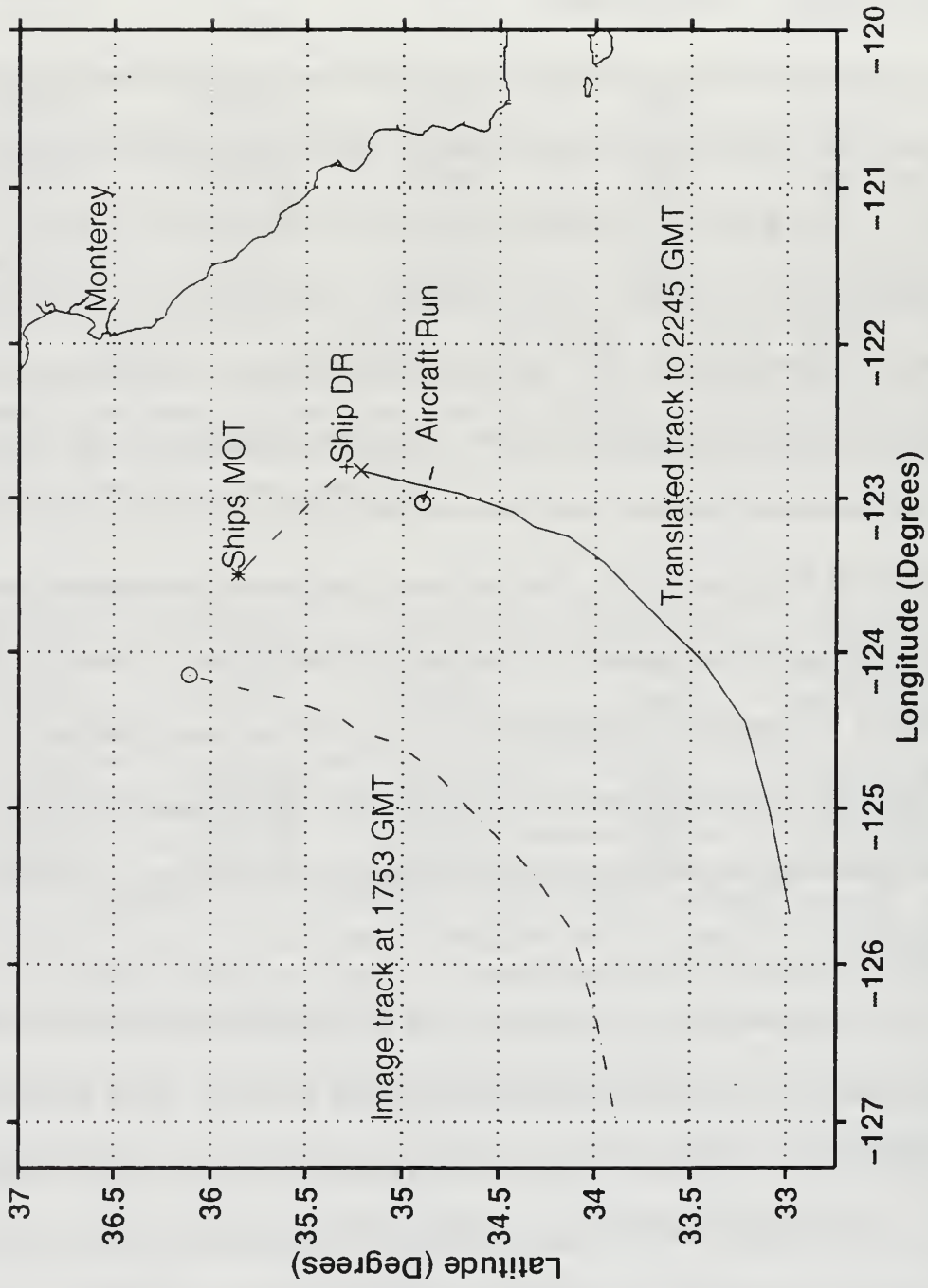

Figure 6 The original satellite position and the translated position of the shiptrack for Cosco Tai He, in-cloud and cross track run 6.

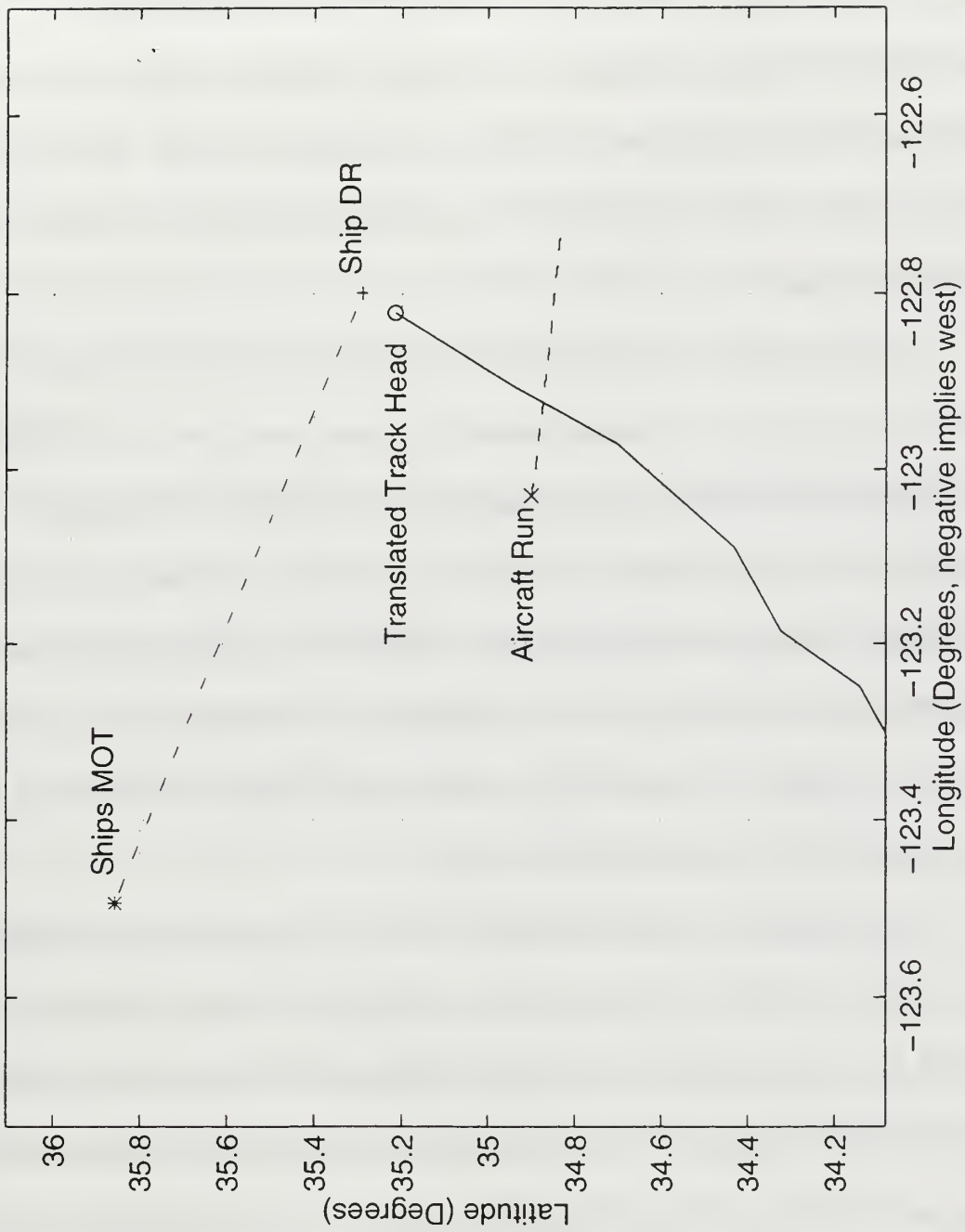

Figure 7 A close up view of the translated shiptrack, the ships route from the last mark-on-top position until the time of the aircraft run, and the aircraft run with the starting point designated by the X.

shiptrack and aircraft data, but serves as a conceptual aid and quality control device to ensure the actual comparison corrections are oriented properly. After the correction estimates are determined realistic, the aircraft data was converted from one second interval measurements to one km mean values. The conversion is done to allow direct comparison to the satellite data which is in one km square resolution values.

The procedure for converting the data entailed the following steps. An aircraft component speed perpendicular to the track center line was determined using the aircraft heading, aircraft speed, and track heading. The airspeed is then used to convert the aircraft data into the one kilometer bins perpendicular to the track. Also from these parameters, the satellite data matrix is corrected to match the cross track direction flown by the plane. This entailed taking a mirror image of the matrix from left to right for tracks with a right to left direction when facing the track head from down track.

A minimum, one kilometer effective radius, average is designated the center of the aircraft run. The effective radius minimum centers matched the center points determined by the maximum concentration average as predicted by the results from section A. From this interval, the remaining run data are averaged into kilometer bins out from this center point. The composite data is cropped to contain only bins with aircraft and satellite data, the final process to ready the aircraft data for comparison against the matrix of satellite data.

As stated, an aircraft run is not necessarily perpendicular to a track's centerline. Furthermore, it is assumed that the track image-characteristics maintain only relative consistency. Under these conditions, the conservation of the imaged track shape and specific bin brightness to a spatially translated track, with a temporal difference, is unrealistic. Trigonometric offsets to account for the cross track angle and data averaging to make use of the relative consistency of the ship track characteristics are employed to make the translated data comparable.

From the aircraft heading, an offset in the along track direction from the true perpendicular case is determined. For each kilometer bin average of aircraft data, an associated offset is assigned by rounding to the nearest kilometer up or down track from the associated perpendicular position. The aircraft data cross-section is corrected to match the associated satellite data cross-section. Additionally, a five kilometer average of the satellite data for the aircraft associated offset position is performed to minimize the changes in along track character and shape over the translation period. Averaging schemes were evaluated using from single bin satellite data values to 10 bin averages. A five bin average was chosen since use of averages greater than five bins increasingly washed out satellite reflectance changes and use of less than 5 bins did not significantly reduce the noise.

The next phase of the analysis is to compare the two data sets and determine the fractional change relationship between effective radius and reflectance. Several strategies have been applied to match these data sets and minimize the noise. However, the cross track kilometer bin values have fractional changes that only relatively correspond to the satellite data due to both temporal and spatial displacements. To minimize these affects, the runs are apportioned into three regional averages which will be used in the evaluation of the fractional change ratio. The averaged run regions consist of a before peak average, peak average, and after peak average, where the peak signal is a shiptrack.

The following criteria were applied to select the averaging regions. First, areas of transition between the zones would not be included since the satellite detected track width and aircraft width will differ due to the different functions of the sensors and different resolutions. The zones are determined across intervals of corresponding trend between the data sets where increasing (decreasing) reflectance corresponds to decreasing (increasing) effective radius. Along with these limitations, the image data reflectance values and aircraft tracks must be discernible against the background. The final criteria was that the each of the averaged data bins must have more than 50% of all data points within the LWC range of 0.05 to 0.20 g/m^3.

The second, third, and fourth criteria eliminate 3 of the nine runs that initially appear to be reasonable cases. All three cross track runs on the Hanjin Barcelona are eliminated. The first run shows no corresponding trend, in that reflectance is very dynamic and the effective radius is nearly constant. The second and third runs are toward the end of the detectable image track. The second run's satellite data has no appreciable signal while the third run lacks sufficient data points, within the liquid water constraints, to fill many of the one kilometer bins.

Appendix A presents the evaluated data for the six remaining Cosco Tai He cases. The plots include the aircraft measured one km interval data and the zonally averaged values for reflectance and effective radius. The comparison of the three averaged values in each run produce three fractional change pairs per run for a total of eighteen fractional change pairs.

The relationship to examine these cases is based on Equation 11 and can be written as

$$\frac{\Delta \overline{r_{eff}}}{\overline{r_{eff}}} = D \frac{\Delta \overline{\rho_{(3.7)}}}{\overline{\rho_{(3.7)}}} \qquad 15$$

since both data sets use averaged discrete data. Equation 15 relates the fraction change of averaged reflectance to the fraction change of averaged effective radius where D represents the theoretical value of -1 from Equation 11.

Figure 8 shows a graph of the fractional change of reflectance verse the fractional change of effective radius. The data points are clustered into three groups representing the three regression pairs. The pairs are; 1) the before peak to peak characterized by decreasing effective radius and increasing reflectance; 2) peak to after peak showing increasing effective radius and decreasing reflectance and; 3) before peak to after peak with nominal changes in either direction. The regression value of -2.0029, equivalent to $1/D$ from Equation 16 has a standard deviation of 0.15776 over eighteen data points. Equation 11 can now be rewritten as

$$\frac{\partial r_{eff}}{r_{eff}} = -\frac{1}{2.0029}\left(\frac{\partial \rho_{(3.7)}}{\rho_{(3.7)}}\right) = -0.499\left(\frac{\partial \rho_{(3.7)}}{\rho_{(3.7)}}\right), \qquad 16$$

and substituted into theoretical Equation, 12.

The deviation from the theoretical value of D=-1 is expected since the negative one is a linear approximate of what is more likely a non linear function.

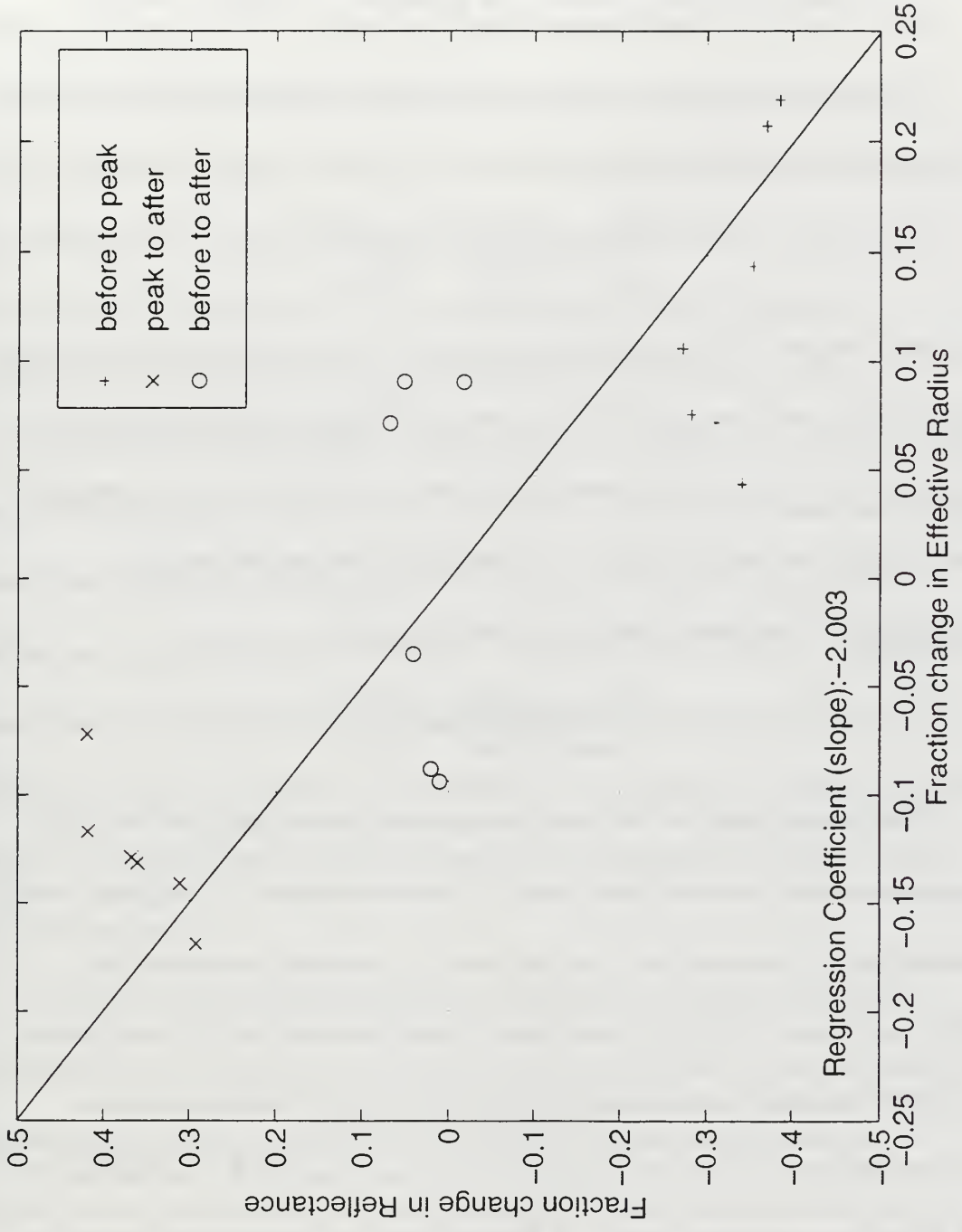

Figure 8 The fractional change of reflectance verse the fractional change of effective radius for the Cosco Tai He.

C. THE FRACTIONAL CHANGE OF DROPLET NUMBER VS THE FRACTIONAL CHANGE OF TRACK WIDTH

The final relationship of the model equation is completed across the first two steps of the theoretical Equation 12

$$\frac{\partial \sigma_y}{\sigma_y} \propto \frac{-\partial CCN}{CCN} \propto \frac{-\partial N_d}{N_d}. \qquad 17$$

The measurement of cloud condensation nuclei was not available for this study. This limitation requires that FSSP data be used to approximate the droplet concentration, where each droplet results from one CCN aerosol. Using this approach, the fractional change in total concentration can be used to approximate the fractional change in droplet number,

$$\frac{\partial(\text{concentration})}{\text{concentration}} \cong \frac{\partial N_d}{N_d}. \qquad 18$$

The data set used in the overall regression process includes the FSSP concentrations and the associated times of measurements. The shiptrack width is detectable in a cross-section as an increase in concentration above the background values. The process of determining the track width is subjective and criteria limiting the runs used was implemented to remove the most indiscernible cases. Each cross track run was hand analyzed to determine the track width as a function of time. If the track was not well defined above the background concentration, or if multiple tracks were apparent in the data, the

run was not used. Figure 1 shows multiple tracks in close proximity and crossing, illustrating the complexity of isolating tracks.

The data set was further limited to only ships with multiple runs so relative fractional changes could be calculated. Averaged data was not useful in this analysis since it created tails outwards from the track peak. These tails varied greatly in extent based on the difference between the peak and background concentrations. Raw data, although noisy, was utilized since it provided a clearly defined region of minimum concentration on the edges of the peaks. The minimums at the edges of the track's concentration peak are within noise of the background concentration, but are clearly part of a guassian distribution of particles across the track. The positions of the track edges have been chosen by finding the most apparent minimum between the peak and background values. Appendix B includes the cross-sections and analyzed edges used in the determination of the fractional change relationship of track width and concentration.

The time interval determined across the peak, from edge to edge, is converted to a perpendicular cross track distance using the aircraft's speed. This standardization of the width intervals from time to distance permits the comparison of runs needed to derive the fractional changes in track width.

The fractional along track changes of integrated concentration above the background value should be zero if dispersion is the only mechanism affecting

the concentration. The conservation of particles across a track indicates the dispersive widening of the track will result in a decrease in peak reflectance. For this reason, the detected peak concentration should correlate to the track dispersion. Since previous sections of this chapter show the reflectance to be a function of concentration and dispersion only implies the conservation of particles, Equation 18 can be rewritten as

$$\frac{\partial \sigma}{\sigma} \cong \frac{-\partial(\text{peak concentration})}{\text{peak concentration}}, \qquad 19$$

for our regression analysis.

Twelve pairs of data are defined by comparing data runs along the same track and only to the following crossing run down the track. Figure 9, a preliminary look at the track width over time, shows the width increasing. The concentration values can not be evaluated in the same manner since different ships inject different types and amount of aerosols into the environment which implies the lack of any correlation in concentration values between ships. However, the fractional changes in concentration are comparable and should be consistent no matter what the initial concentration if dispersion is the only mechanism changing the values. The regression of the fractional change in peak concentration to the fractional change in width can be evaluated, Figure 10, by Equation 19 and yields the relationship

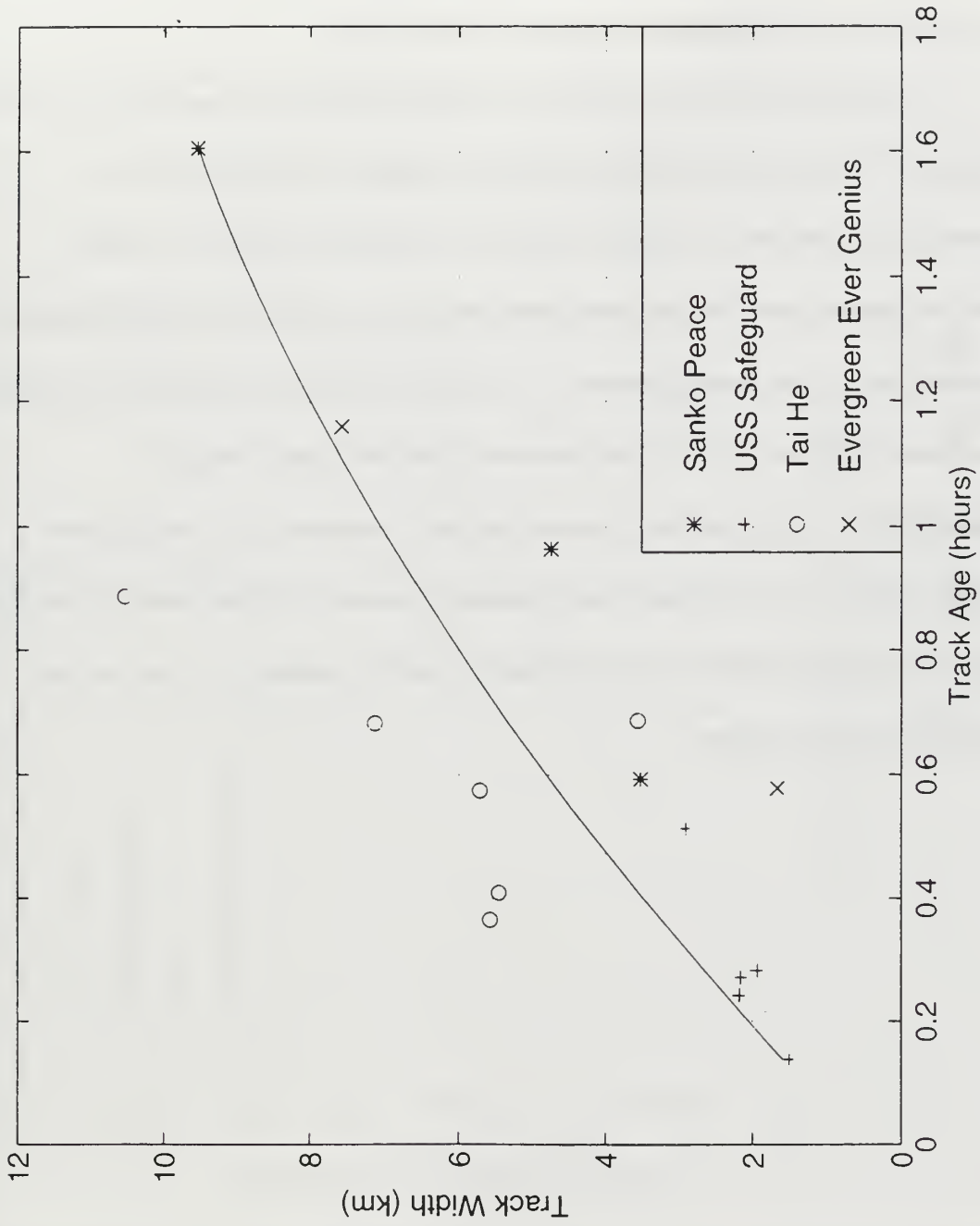

Figure 9 An illustration of increasing track width over time. Time zero is the time of the emission from the ship.

$$\frac{\partial \sigma_y}{\sigma_y} = \frac{1}{0.23205}\frac{\partial N_d}{N_d} = 4.3094\frac{\partial N_d}{N_d}, \qquad 20$$

not the decreasing regression value of -1 as expected.

To explain the departure from theoretical model, the positive value of the fractional change in concentration must be examined since the width is increasing as expected. The age or time since emission of the data points indicate the runs are near the track head positions and imply that the boundary layer may not yet be homogeneous. The continued mixing within the boundary layer could explain the lack of a decrease in the fractional change of concentration, as expected in a dispersion only scenario, by the addition of aerosol. However, as valid as this argument appears with the data set, it will be shown in Chapter V that cloud reflectance is not decreasing as expected for periods of up to six hours.

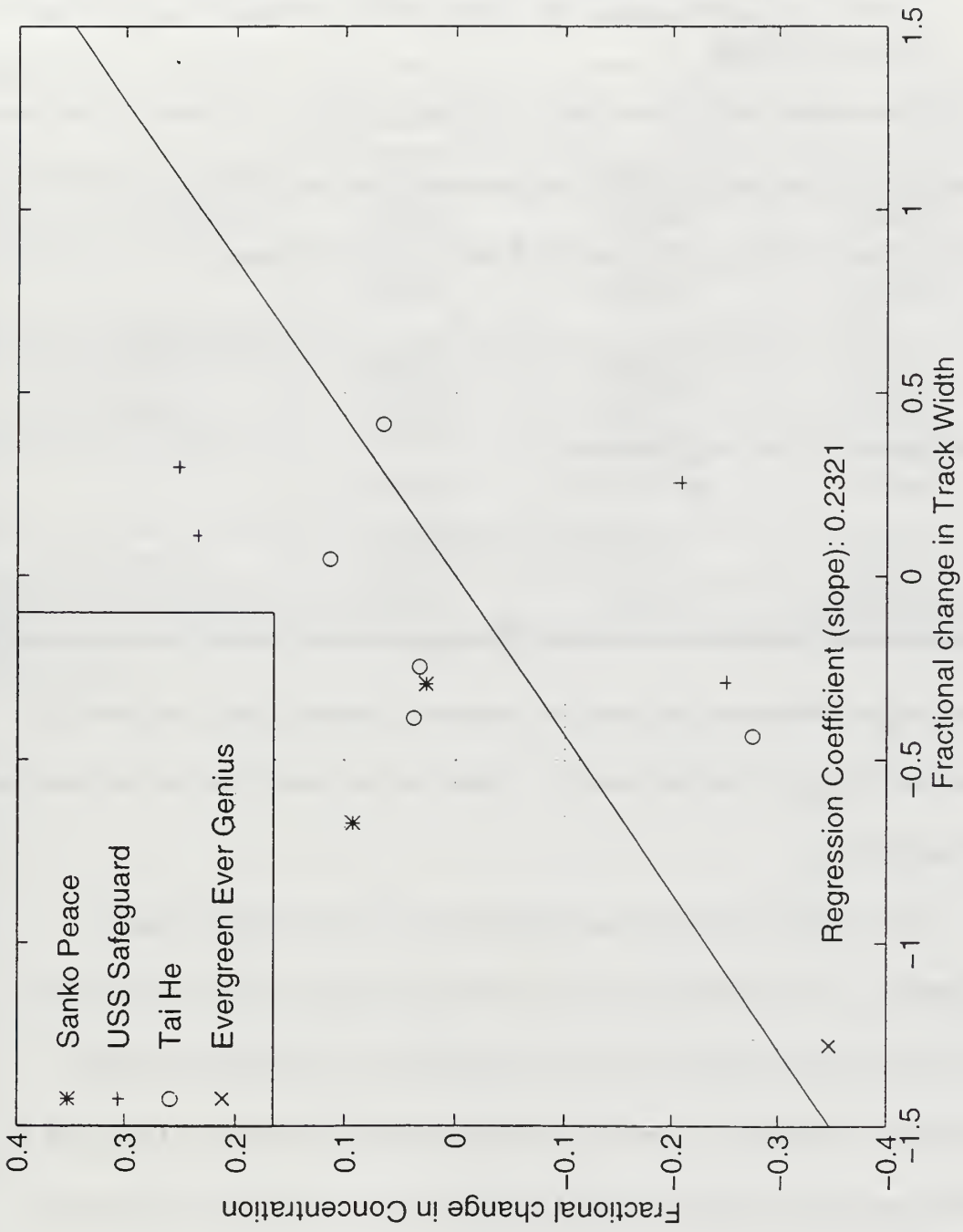

Figure 10 The fractional change in peak track reflectance verse the fractional change in track width.

D. THE CUMULATIVE THEORETICAL FRACTIONAL CHANGE OF SATELLITE REFLECTANCE VS THE FRACTIONAL CHANGE OF TRACK WIDTH

The theoretical proportionality relationships from Equation 12 have been determined, using insitu aircraft measurements and satellite data, in the previous three sections. The analysis resulted in the following,

$$\frac{\partial \sigma_y}{\sigma_y} = (4.31)\frac{\partial N_d}{N_d} = 4.31*(-3.10)\frac{\partial r_{eff}}{r_{eff}} = -13.4*(-0.499)\frac{\partial \rho_{(3.7)}}{\rho_{(3.7)}}, \qquad 21$$

giving an overall process equation of

$$\frac{\partial \sigma_y}{\sigma_y} = 6.667\frac{\partial \rho_{(3.7)}}{\rho_{(3.7)}}. \qquad 22$$

As illustrated in the previous section, the dispersion only model is inadequate to describe the relationship between the fractional change in track width to the fractional change in particle number. Therefore, the models overall solution is also inadequate.

Table 4 shows the statistical significance of the fractional change relationships. The relationship of the fractional change in track width to the fractional change in particle number is the process with the least statistical confidence. However, the certainty of the proportional nature of the width to droplet concentration relationship, in opposition to the negative relationship predicted by the dispersion only theory, indicates there are more processes than just dispersion occurring. This conclusion is further validated through a

comparison of these results to the composite satellite width to satellite reflectance data set (Chartier, 1994) in the next chapter.

Relationship variable	$\frac{\partial \sigma_y}{\sigma_y} = B\frac{\partial N_d}{N_d}$	$\frac{\partial r_{eff}}{r_{eff}} = C\frac{\partial N_d}{N_d}$	$\frac{\partial r_{eff}}{r_{eff}} = D\frac{\partial \rho_{(3.7)}}{\rho_{(3.7)}}$
Number of data points	**12**	**6628**	**18**
Regression coefficient (1/B) (1/C) (1/D)	**0.23205**	**-0.32248**	**-2.0029**
σ (regression coefficient)	**0.11202**	**0.00146**	**0.30346**
Intercept	**0.02902**	**-0.00046**	**0.0272**
σ (Intercept)	**0.05601**	**0.00039**	**0.0372**
Correlation coefficient	**0.54797 moderate**	**-0.93847 very strong**	**-0.85521 strong**
σ (data set)	**0.17671**	**0.03188**	**0.15776**
Random Probability	**6.511%**	**0%**	**.0006105%**

Table 4 A summary of the statistical significance of the three derived regression relationships.

V. COMPARISON TO PREVIOUS ANALYSIS

A. THE DATA SET

In 1995 a composite analysis of shiptracks from the MAST experiment was completed (Chartier, 1995). Chartier's data set of 131 shiptracks, encompassing the satellite data used in this analysis, has under gone the processing described in Chapter III. The first of two data sets used in this comparison are the ten kilometer averages of extracted track widths. These track widths were automatically extracted from the images using the Nielsen and Durkee (1992) algorithm and averaged to reduce noise. The other data set are the peak reflectance values at 3.7 μm for the 131 shiptracks.

As Chartier discusses, the noise level within the runs is high. Differing from his technique, the reflectance and width data for each run used in this study is smoothed using a sixth degree polynomial fit. Each smoothed track generated is converted from a function of distance to a function of time using the relative wind speed. The run data is now represented by reflectance and width values, extracted at 15 minute intervals, from the polynomial fit. The 131 processed data runs are then combined to form the composite data set.

A smoothed composite width is then defined by a second sixth degree polynomial fit. Figure 11 displays the first fourteen hours of the width data. Data beyond 14 hours is sparse.

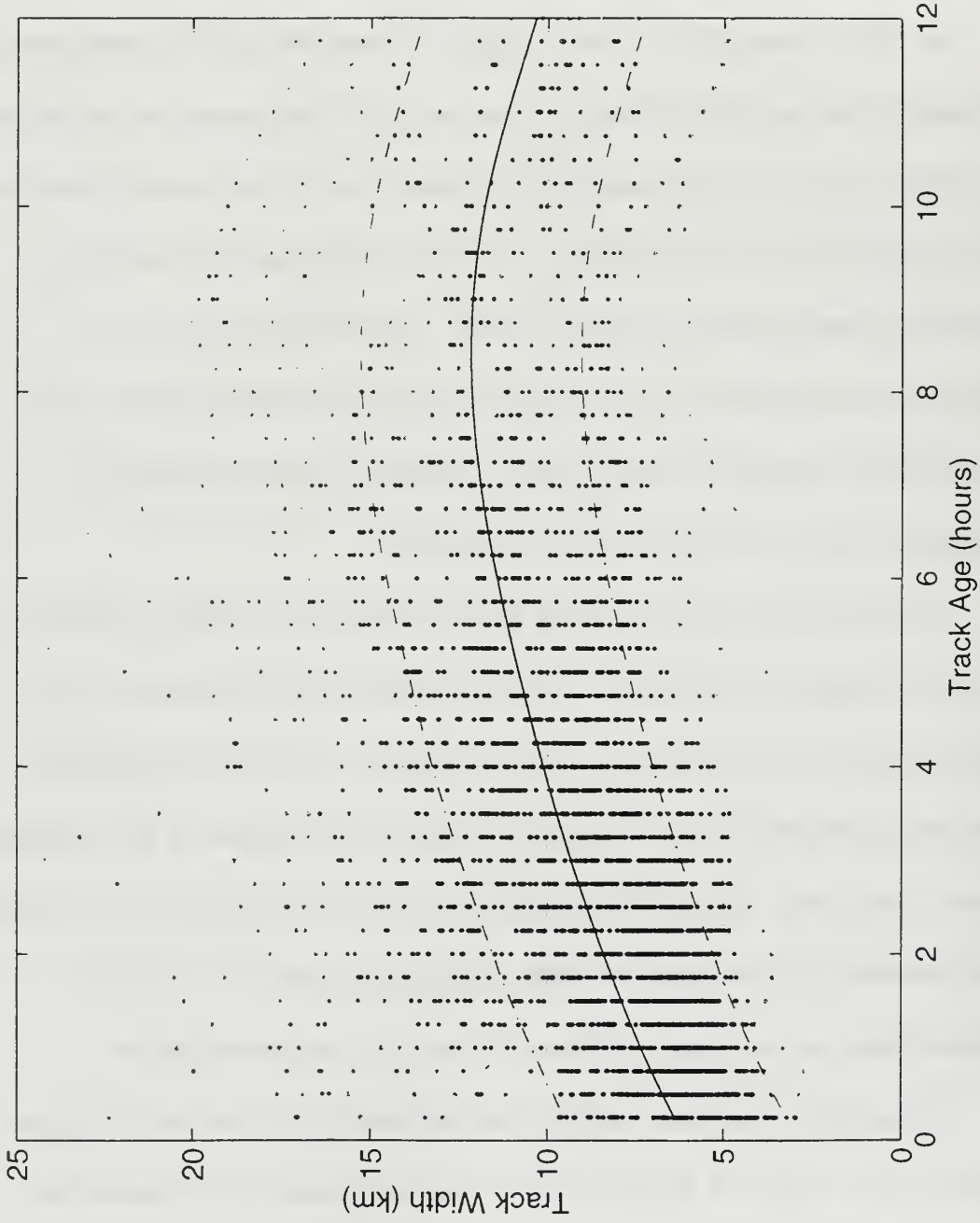

Figure 11 Sixth degree polynomial fit of 131 smoothed track widths, solid line, versus time. The 131 individual runs are represented by the dotted series

A look at the change in track width with time shows the width increasing for the first six hours. Figure 12 shows a decrease in satellite detected widths occurs as the reflectance falls below the detectable reflectance resolution from the background. In the first six hours, the increasing width follows the aircraft data width increase, even though the magnitude may not be the same.

In Figure 13, the smoothed peak reflectance over the first 14 hours varies between 14% and 15% reflectance. This data does not follow a specific trend and the fractional change in reflectance over time is characterized by slight variations from zero. The lack of fractional change in reflectance further illustrates the departure from the theoretically expected decline in peak reflectance due to the dispersion only assumption.

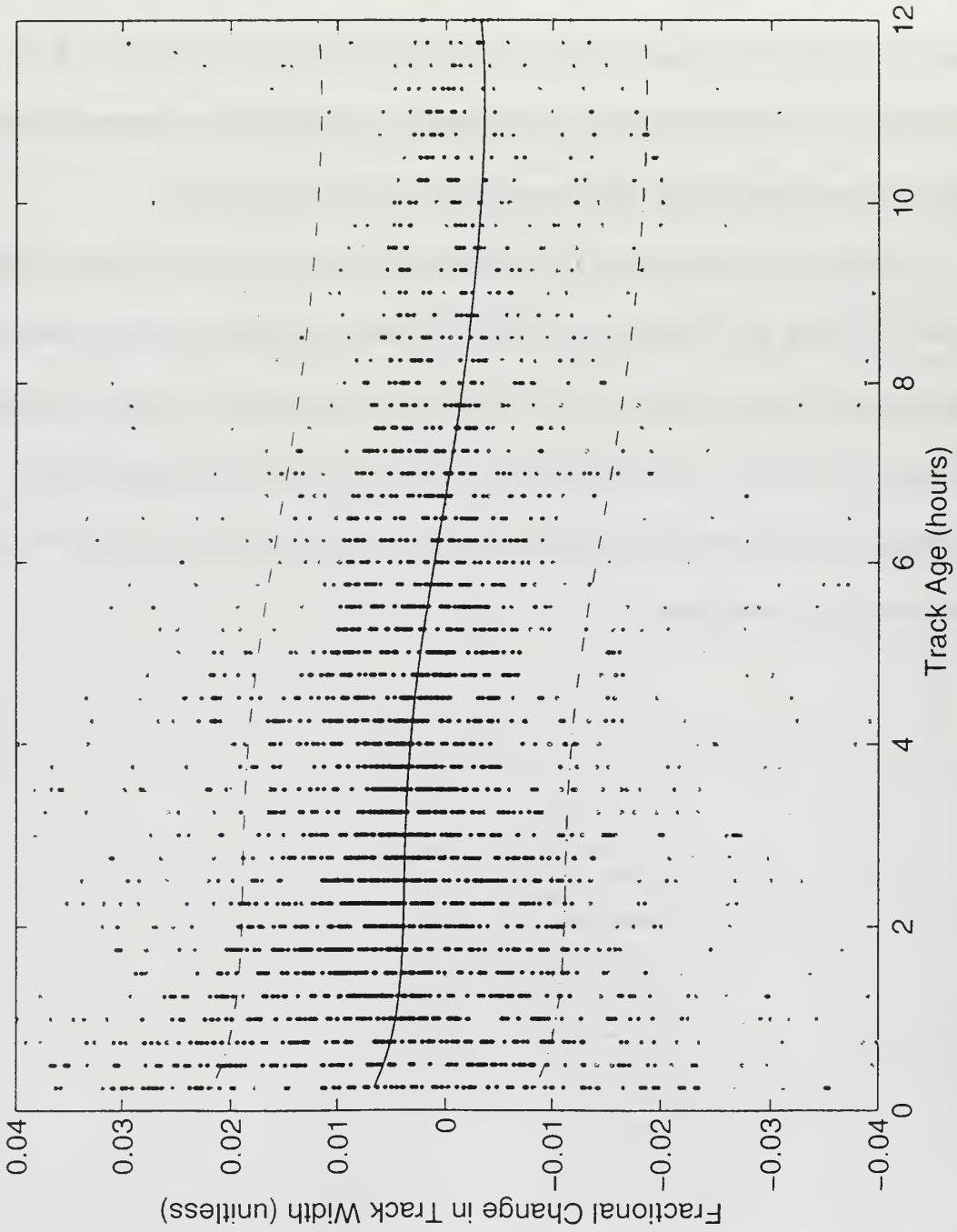

Figure 12 Sixth degree composite fit of the fractional change in track width, solid line, verse time. The fractional changes in track width for the 131 individual runs are represented by the dotted series.

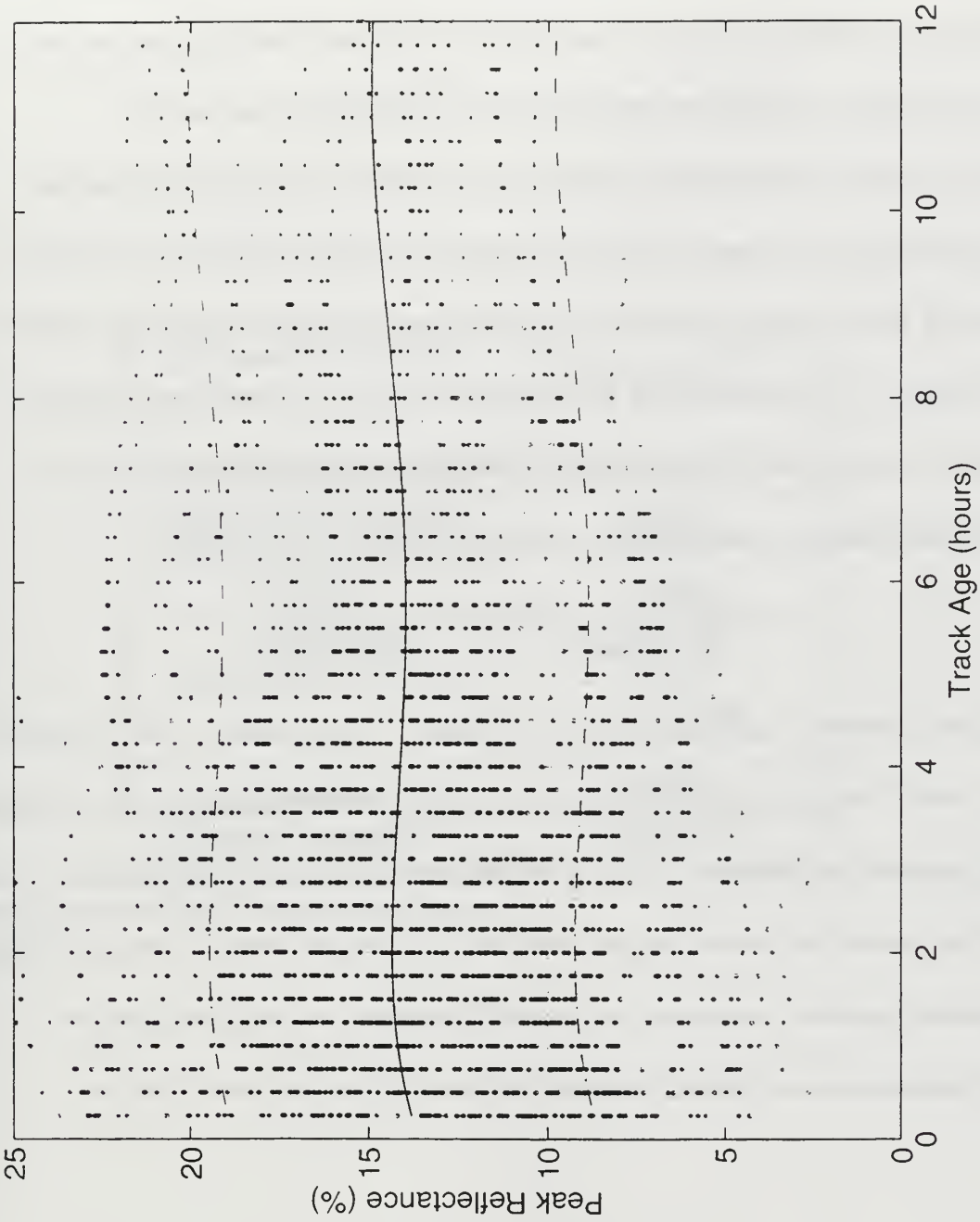

Figure 13 Sixth degree composite fit of smoothed peak reflectance, solid line, verse time for 131 averaged tracks. The 131 individual run reflectance values are represented by the dotted series.

B. THE COMPARISON OF RESULTS

The first six hours of satellite data are consistent with the aircraft data increasing width and nearly constant peak reflectance. For the shorter period aircraft data, a plausible argument that the Marine layer may not be homogeneous is considered. However, the six hour trends observed in the composite data set discount the non-homogeneous boundary layer reasoning since the time scales for turbulence within a mesoscale boundary layer are of one hour or less. In short, the long term trends observed substantiate the aircraft results. Comparison of the fractional change in peak reflectance versus the fractional change in width of the smoothed composite data yields

$$\frac{\partial \sigma_y}{\sigma_y} = \frac{1}{0.98342}\frac{\partial \rho_{(3.7)}}{\rho_{(3.7)}} = 1.0169\frac{\partial \rho_{(3.7)}}{\rho_{(3.7)}}, \qquad 23$$

with the statistical significance shown in Table 5. This positive value reinforces the overall fractional change relationship of the aircraft to satellite data, Equation 20. Figure 14 graphically illustrates the theoretical, aircraft/satellite, and satellite overall fractional change relationships. The similarity of the statistically significant positive correlation's of aircraft/satellite and satellite/satellite relationships are conclusively contrary to the negative theoretical value.

Relationship variable	$\frac{\partial \sigma_y}{\sigma_y} = 1.0169 \frac{\partial \rho_{(3.7)}}{\rho_{(3.7)}}$.
Number of data points	**24**
Regression coefficient	**0.98342**
σ (Regression coefficient)	**0.15747**
Intercept	**-0.0034**
σ (Intercept)	**0.00059**
Correlation coefficient	**0.79959** **very strong**
σ (data set)	**0.00098**
Random Probability	**0.000276%**

Table 5 The statistical data for the satellite width to satellite reflectance data from Chartier's (1995) composite data set.

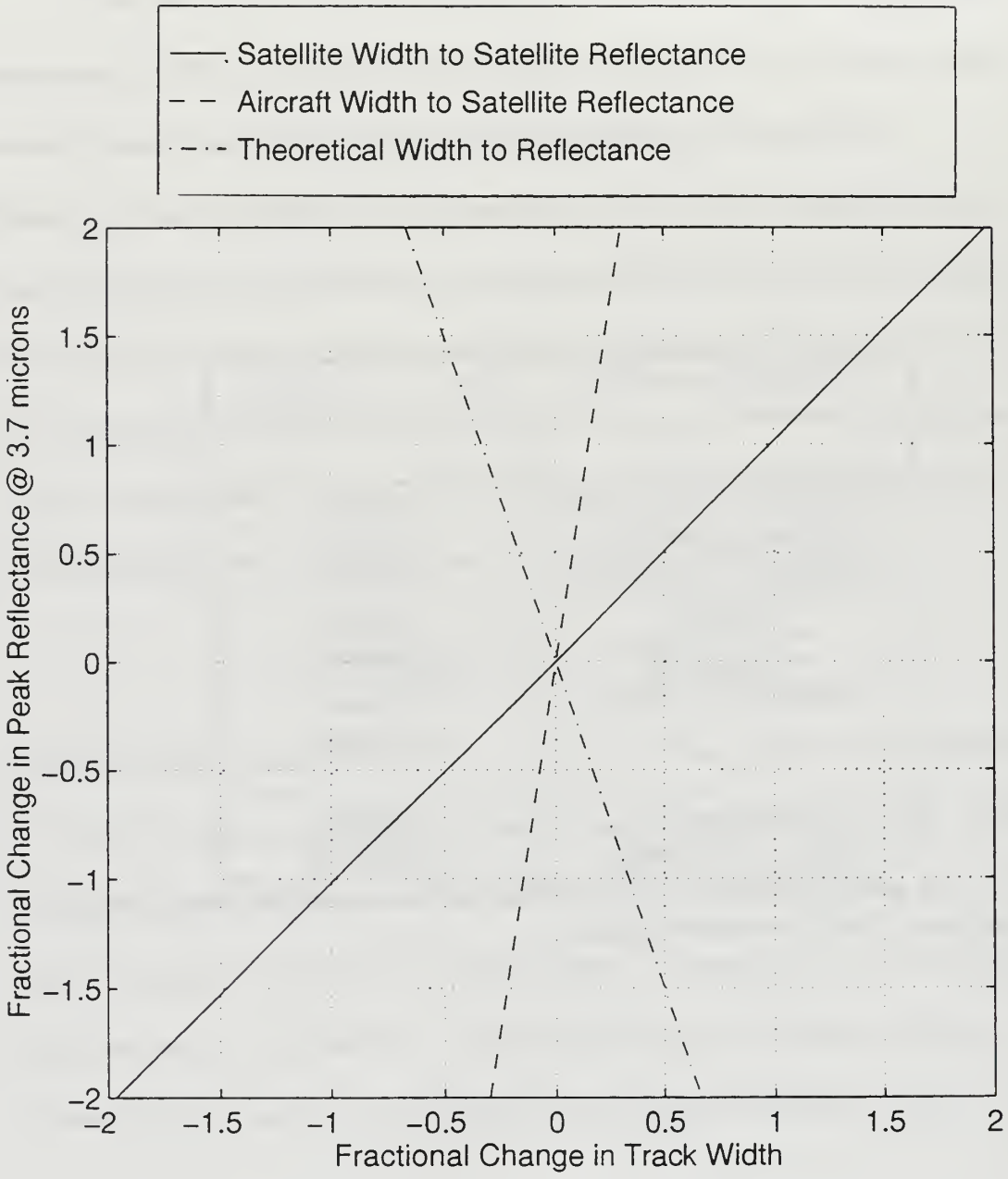

Figure 14 Regression fits of theoretical, aircraft/satellite, and satellite overall fractional change relationships.

VI. CONCLUSIONS AND RECOMMENDATIONS

A. CONCLUSIONS

Deviation from the dispersion only model is evident in the aircraft to satellite and satellite to satellite relationships. This conclusion is evident in the satellite to satellite data comparison only, however, the aircraft data provides a test of the theoretical relationships between track width, droplet concentration, effective radius, and reflectance. The testing of the theoretical relationships indicates the deviation from the dispersion model occurs in the width to droplet concentration relationship.

The departure from the dispersion only model can be explained partially within the confines of the MAST hypotheses. Hypothesis 1.2 states CCN and droplet concentrations modification in the form of increased column liquid water content by the stabilization of the drop size distribution and due to aerosol injection. Gas-to-particle conversion providing down track CCN is a second explanation of the deviation of CCN and droplet concentrations from the dispersion only model (Hypothesis 1.3). A third source, not specifically addressed in the MAST hypotheses, is CCN modification due to repeated cloud evaporation and condensation processes. These cycles will modify the aerosols as they are restructured and mixed while dissolved in the drops. Most likely, it is combination of all three processes and possibly other undetected phenomena.

Most other MAST hypothesis statements do not apply to the test model. However, hypothesis 3.1 can be considered for elimination by the data since the aircraft measured widths show a continued increase not track confinement. The follow-on cloud dynamic hypothesis, 3.2, suggests the track maintains its form due to enhanced vertical motion within the track due to the release of latent heat from condensation. As demonstrated in the aircraft and satellite data, track form is not conserved over time. An approach to further study this evidence is suggested in the recommendations.

In closing, the strong decrease in reflectance under a dispersion only model in not observed. While dispersion is evident by the increasing width of the elevated cloud concentration nuclei values, the effective radius and reflectance at the track center is conserved. This result is significant in limiting the plausible explanations for the long life and unexpected brightness in shiptracks. The examination of the MAST hypothesis, under the scientific method, results in a refined model and hypothesis to examine. The changes in liquid water content and CCN are significant influences on shiptrack brightness, but the data appears to discard the conservation of track form and width. In the following section, recommendations to refine the model further and examine other MAST hypotheses are provided.

B. RECOMMENDATIONS

The objective of this study has been accomplished. However, there are now new questions to answer. The C-130 aircraft measurements utilized in the study were a fraction of the overall data collected during the MAST experiment. In incorporating more data from the C-130, and additional information from other aircraft not available for this study, a more complete model of the fractional change in width to the fractional change in CCN may be developed. Below are my recommendations pertinent to reaffirming the conclusions above and investigating phenomena uncovered but not in the scope of this study.

1. Examine the fluctuations in liquid water content and particle number along the tracks to discern the interaction of these parameters in the enhanced reflectance formula.
2. Integrate the cross-track liquid water content and particle count to verify the addition of particles and liquid water content along track.
3. Examine the MAST Cloud Dynamic hypothesis 3.1 and 3.2, suggesting induced circulations or enhanced vertical motion exist in shiptracks by isolating the measured atmospheric component velocities measured by the aircraft.
4. Incorporate CCN data when available to determine the percentage of hydroscopic aerosol and chemical make up of all aerosols as a function of

time to evaluate the gas to particle conversion and cloud-processes modification theories.

5. Confirm the existence of the non homogeneous, unstable, cloud and track formation region, low LWC region of Figure 4, as a function of FSSP detected liquid water content by observing the non activated aerosol count of small, (0.1 to 3.0μm) diameter particles measured by the passive cavity aerosol spectrometer probe, PCASP.
6. Confirm the existence of the non homogeneous, unstable, cloud and track region with possible coalescence or precipitation, high LWC region of Figure 4, as a function of FSSP detected liquid water content by observing the activated droplet count of the two dimensional optical array probes for 25 to 800μm and 200 to 6400μm diameter drops.

These recommendation will define the shiptrack mechanism responsible for the enhanced long term brightness beyond the shown non-dispersive droplet concentrations.

APPENDIX A. CROSS TRACK EFFECTIVE RADIUS AND REFLECTANCE PLOTS

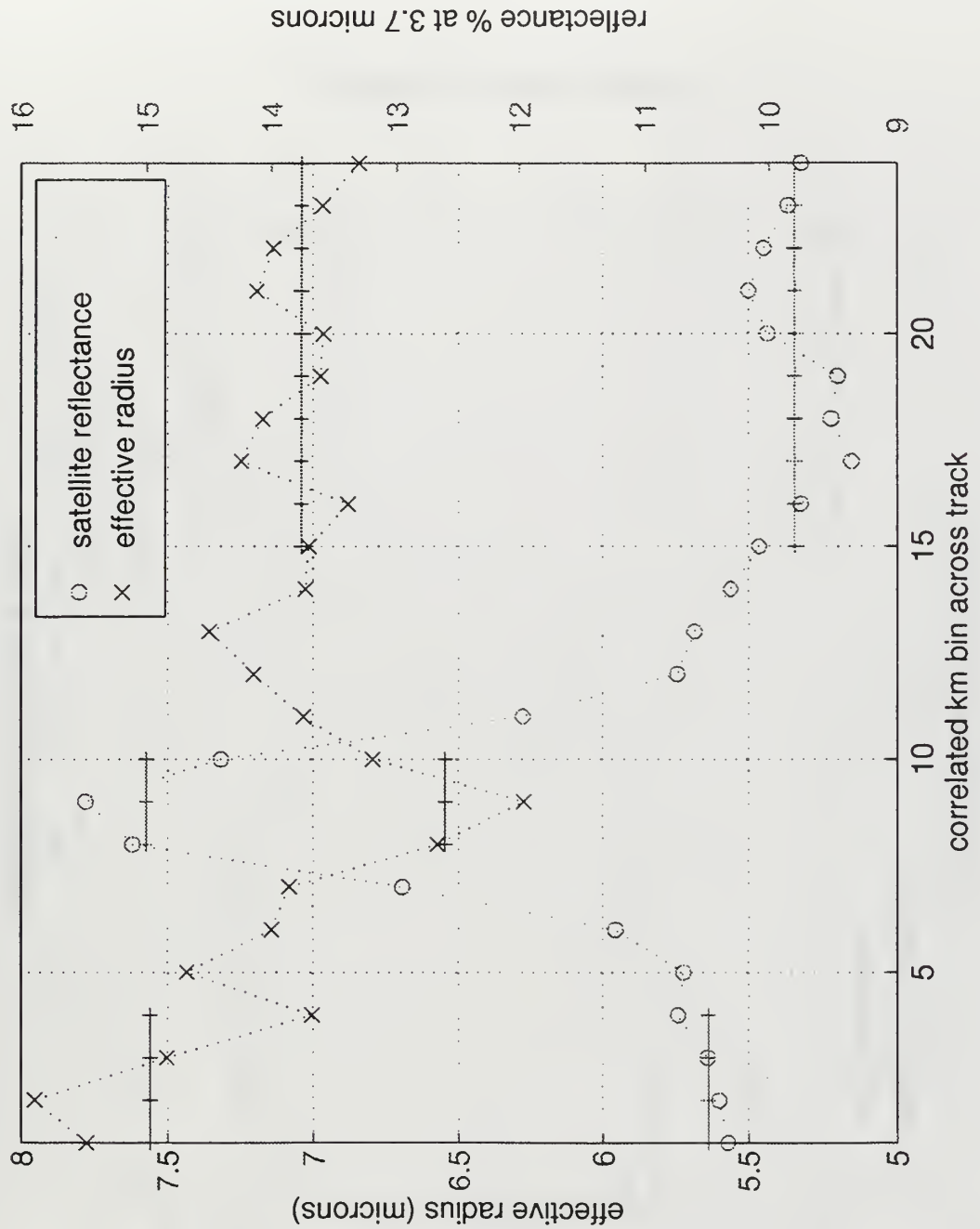

Figure A1 Cross-track plots of one km resolution reflectance values and one km averaged effective radius measurements for flight A346, start time 18:05:40.

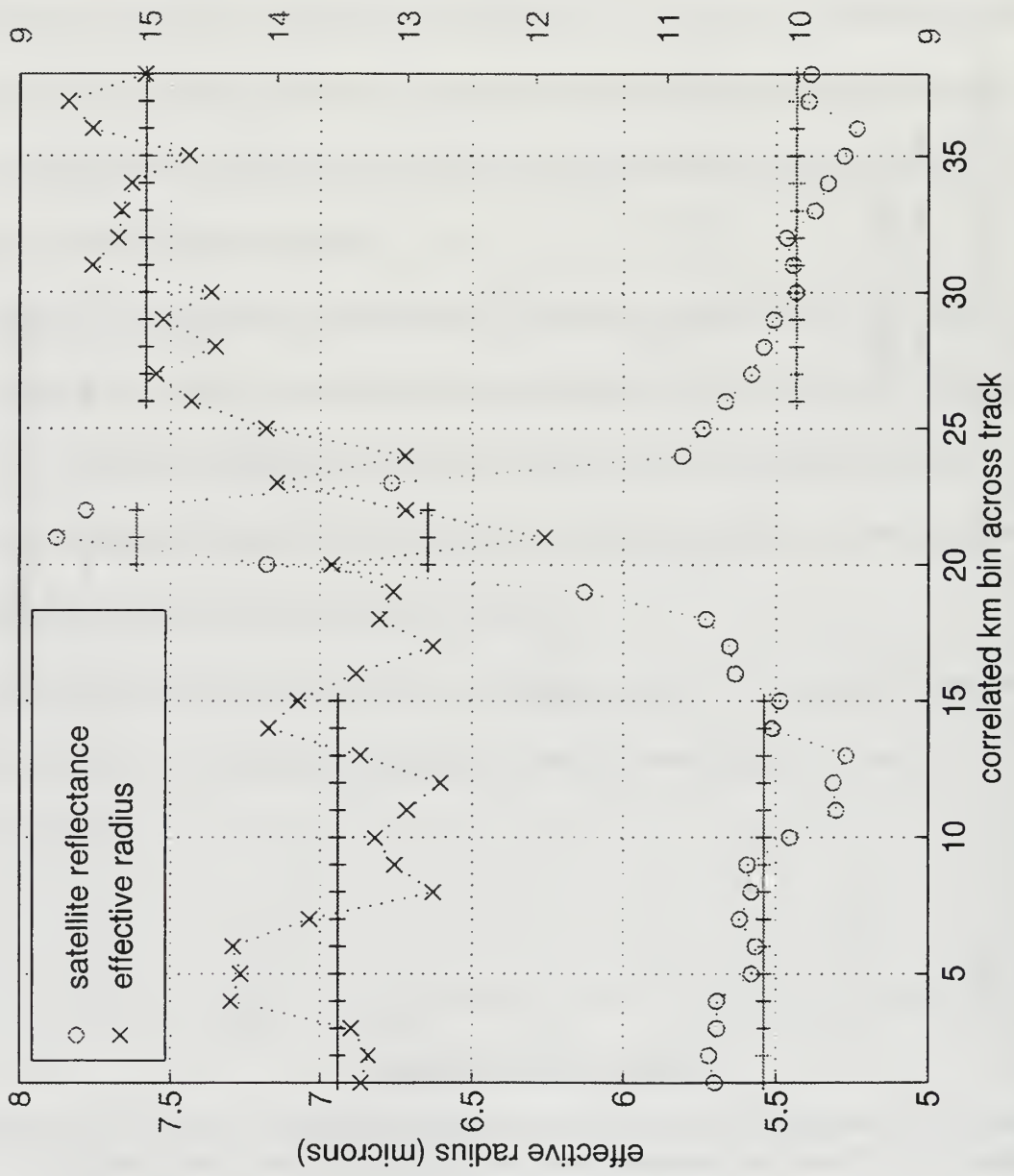

Figure A2 Cross-track plots of one km resolution reflectance values and one km averaged effective radius measurements for flight A346, start time 18:14:52.

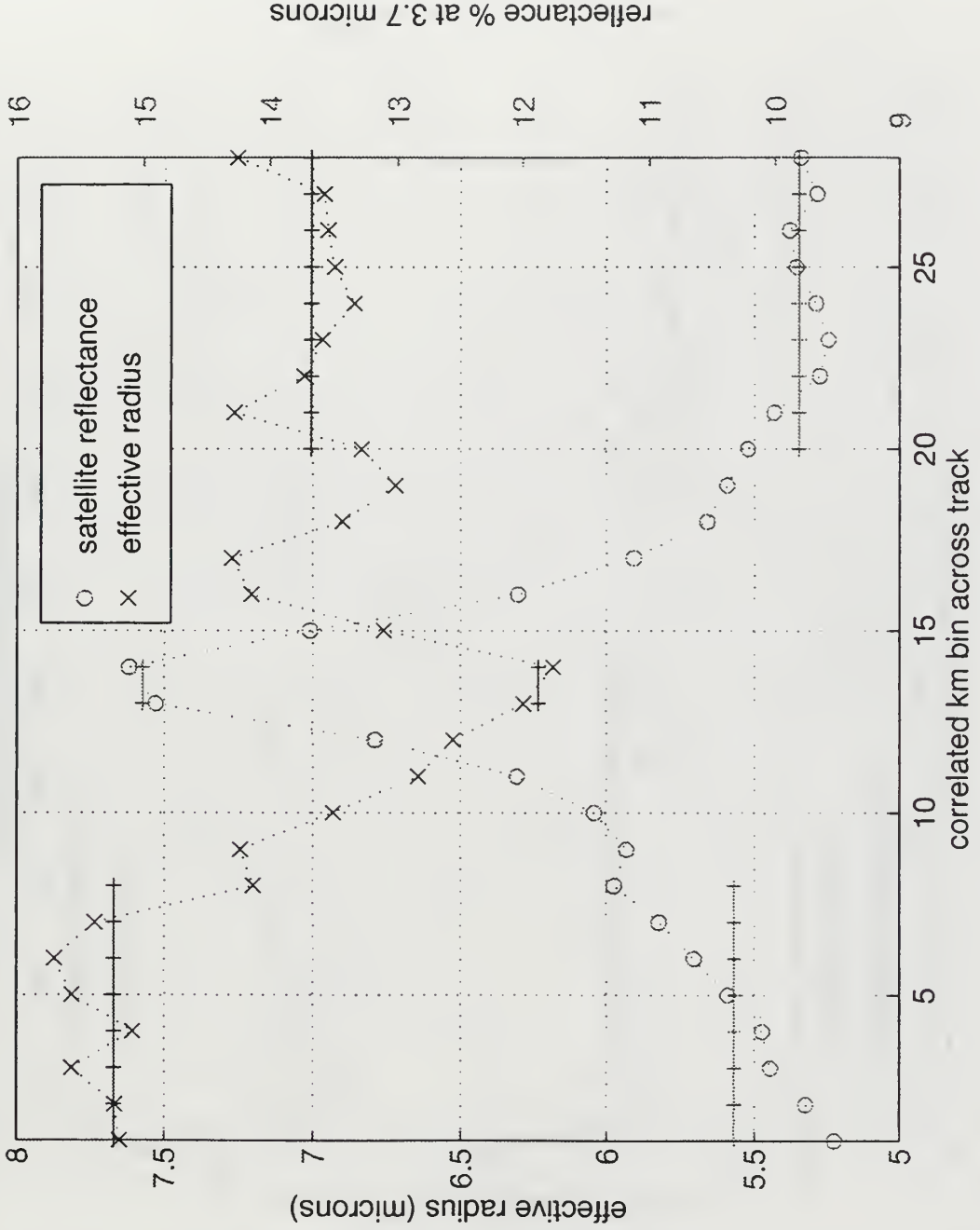

Figure A3 Cross-track plots of one km resolution reflectance values and one km averaged effective radius measurements for flight A346, start time 18:22:42.

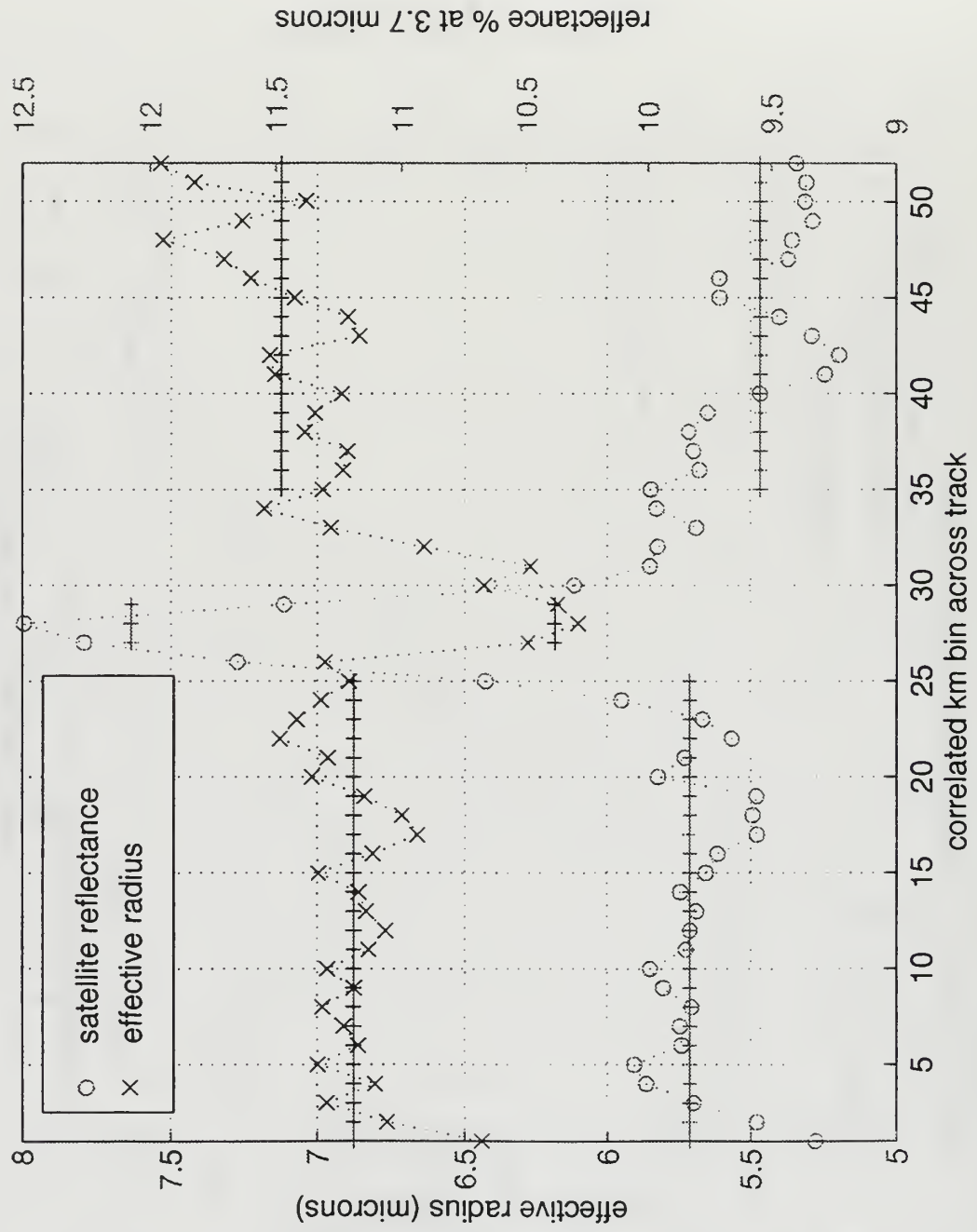

Figure A4 Cross-track plots of one km resolution reflectance values and one km averaged effective radius measurements for flight A346, start time 21:20:13.

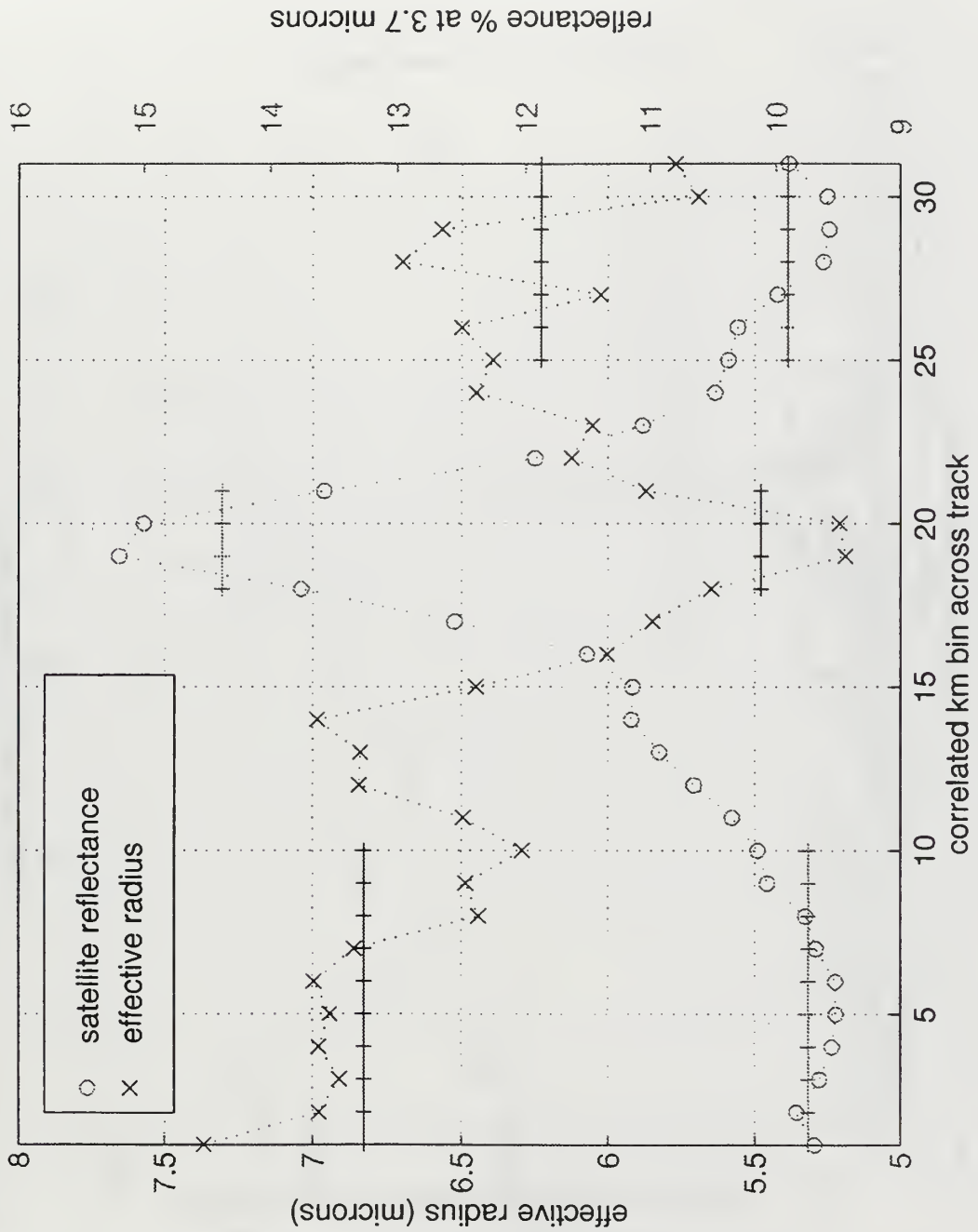

Figure A5 Cross-track plots of one km resolution reflectance values and one km averaged effective radius measurements for flight A346, start time 22:13:47.

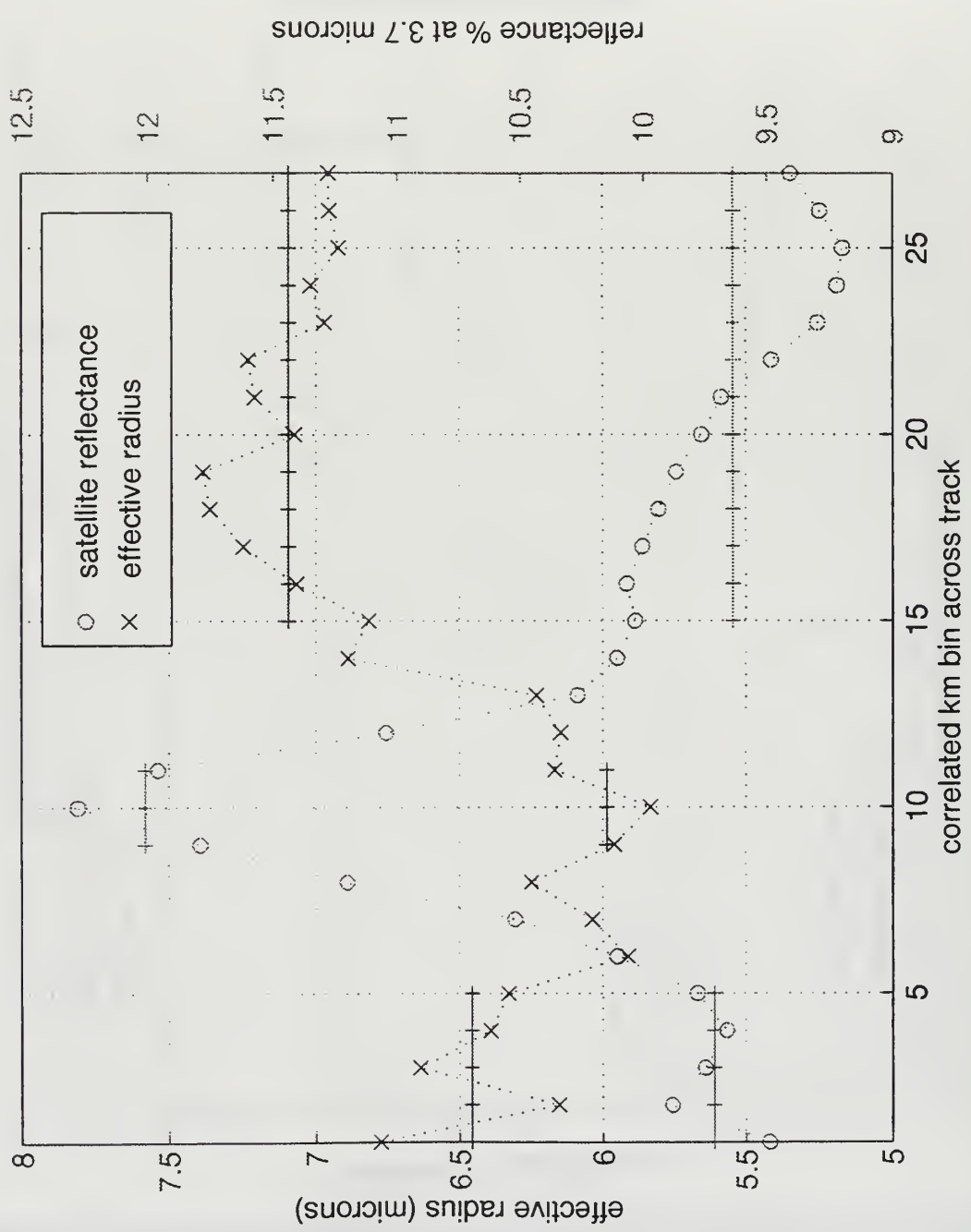

Figure A6 Cross-track plots of one km resolution reflectance values and one km averaged effective radius measurements for flight A346, start time 22:43:08.

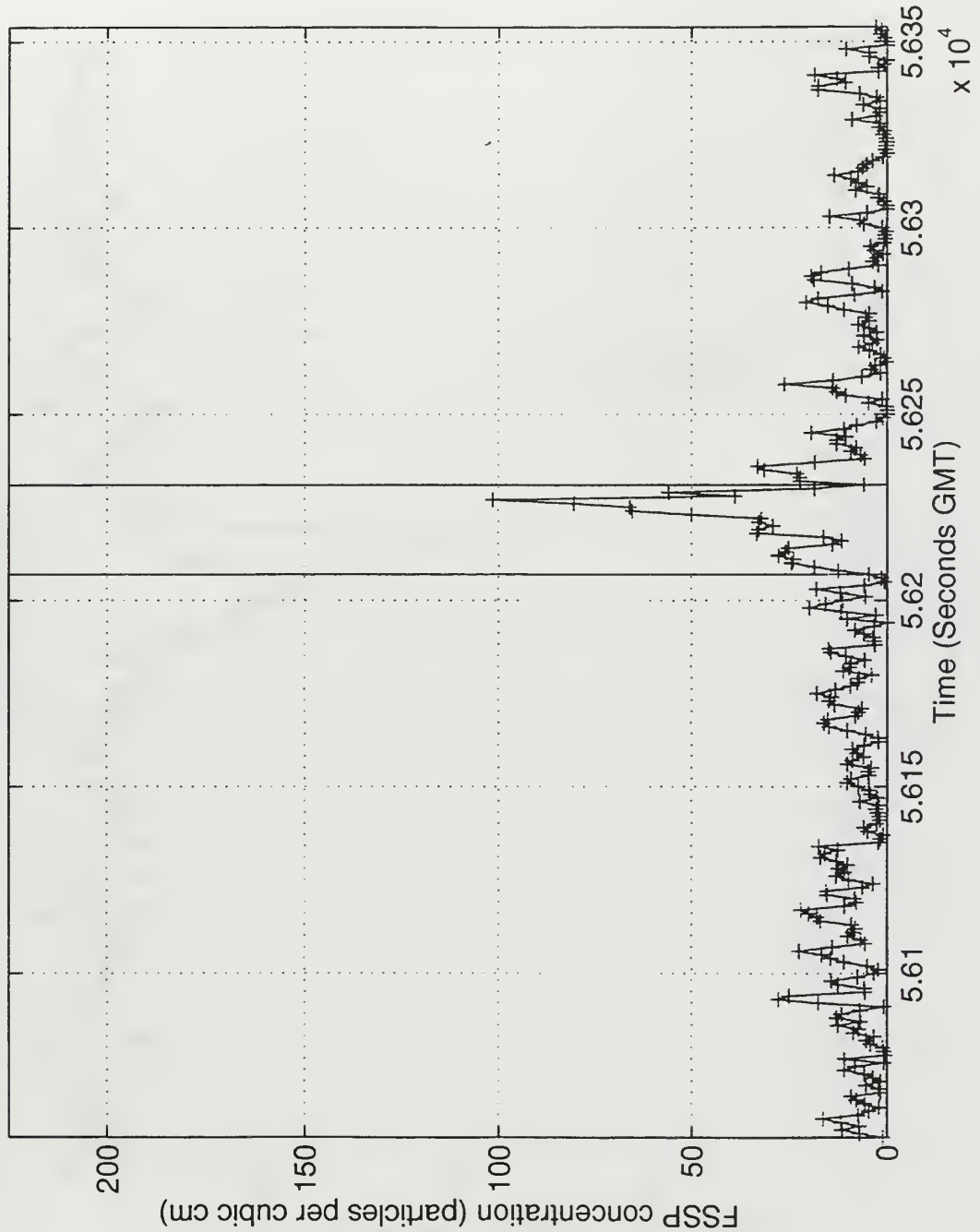

Figure B1 Cross-track plots of the FSSP detected droplet concentration measurements for flight A338, start time 15:34:16.

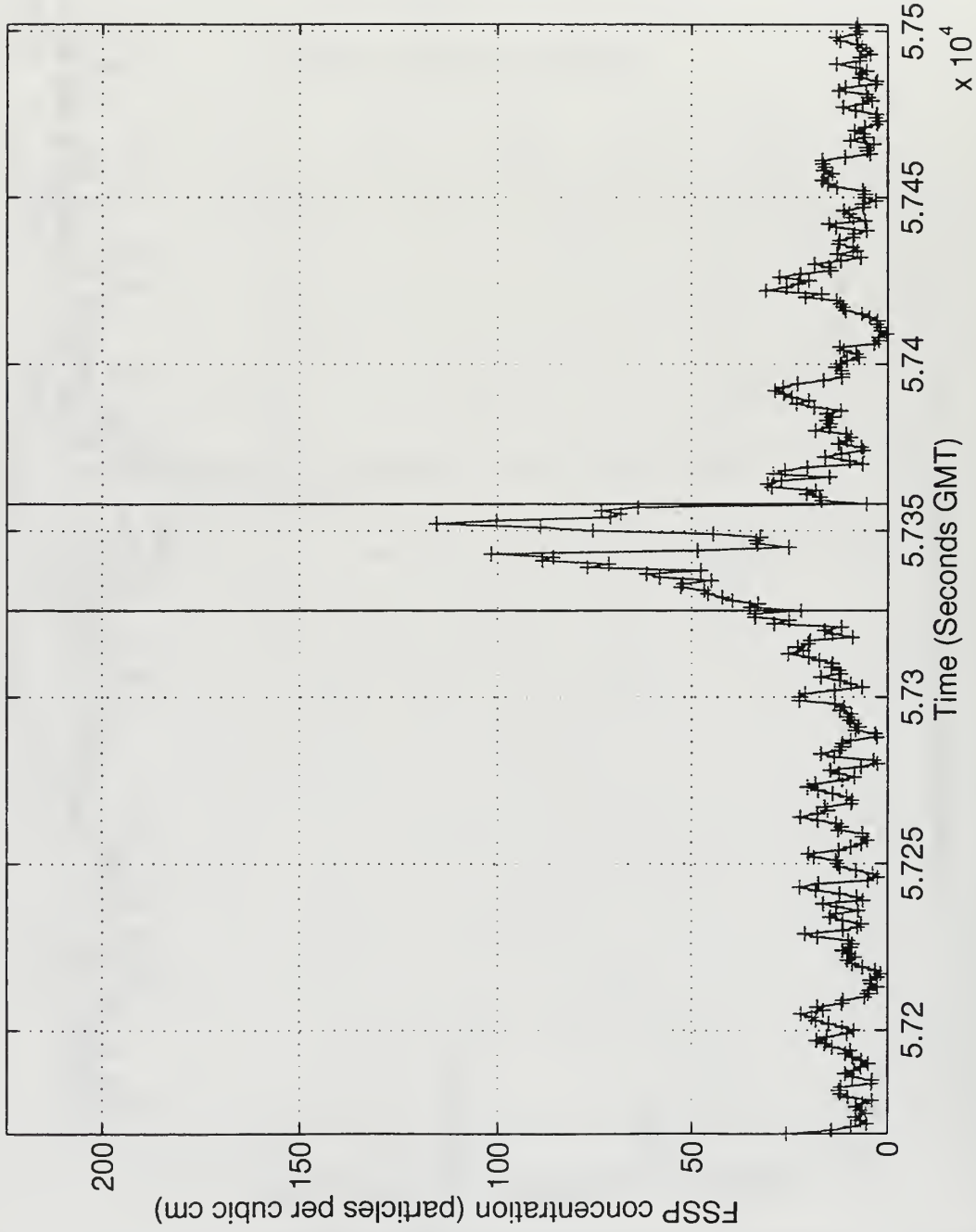

Figure B2 Cross-track plots of the FSSP detected droplet concentration measurements for flight A338, start time 15:52:49.

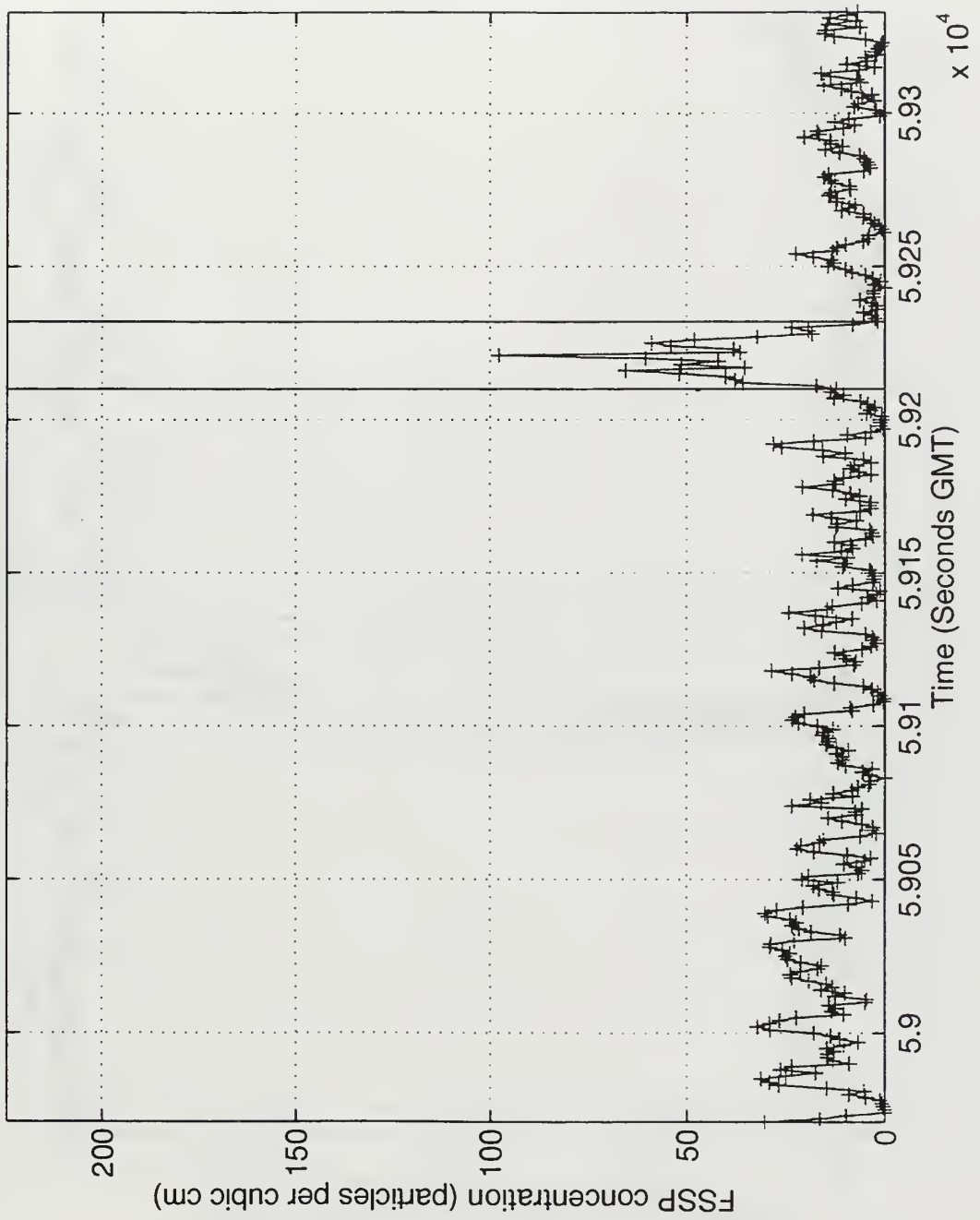

Figure B3 Cross-track plots of the FSSP detected droplet concentration measurements for flight A338, start time 16:22:51.

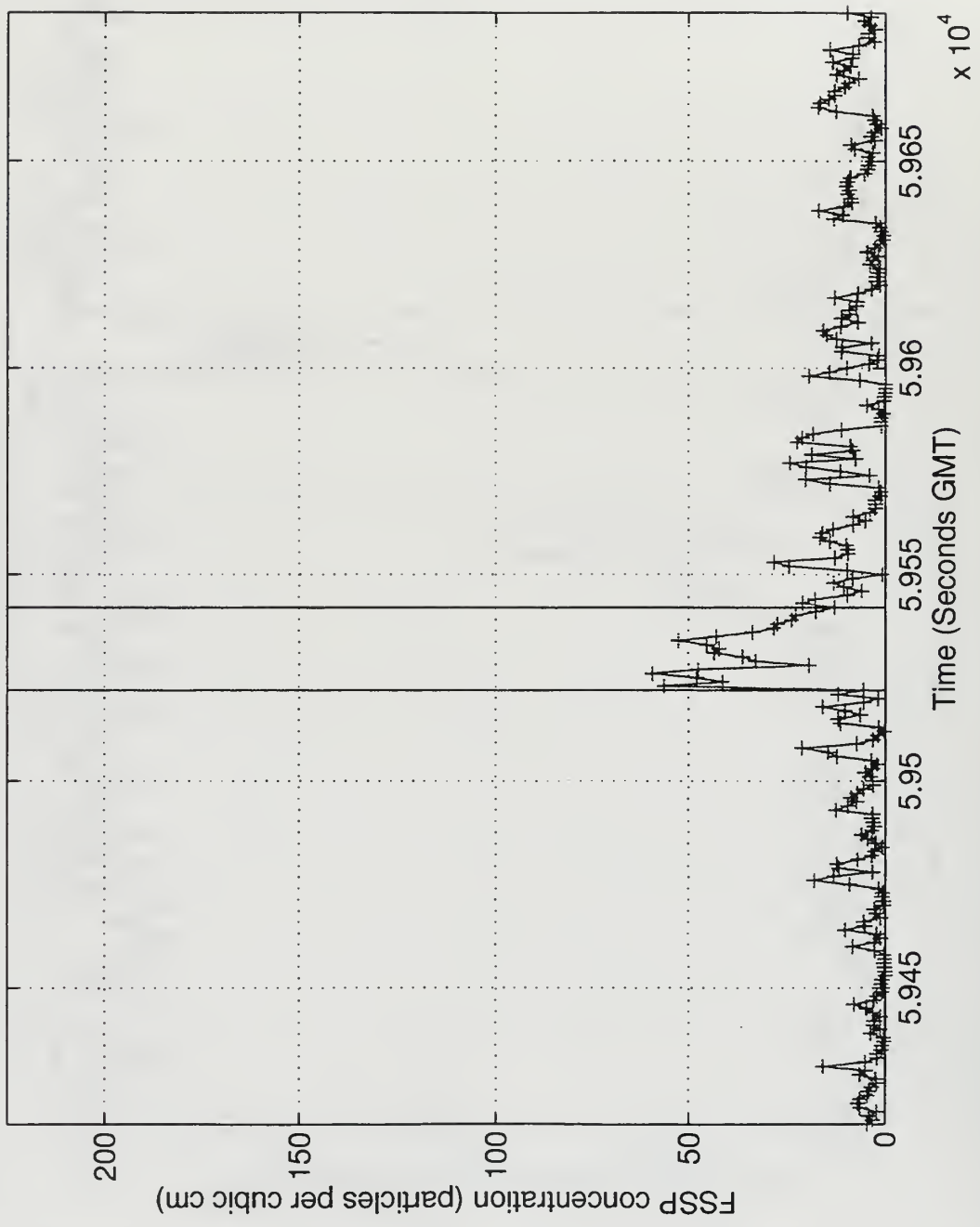

Figure B4 Cross-track plots of the FSSP detected droplet concentration measurements for flight A338, start time 16:30:17.

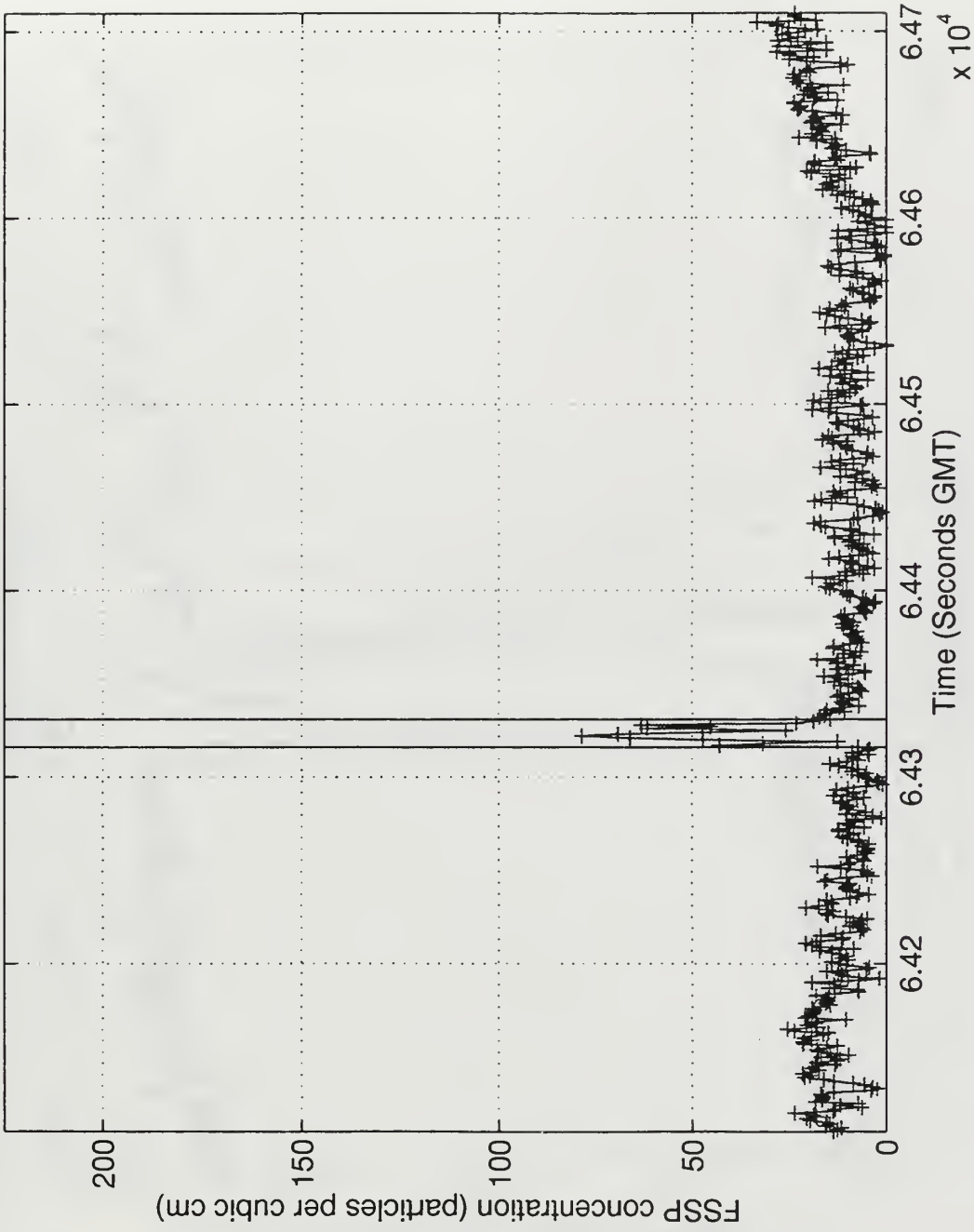

Figure B5 Cross-track plots of the FSSP detected droplet concentration measurements for flight A338, start time 17:48:30.

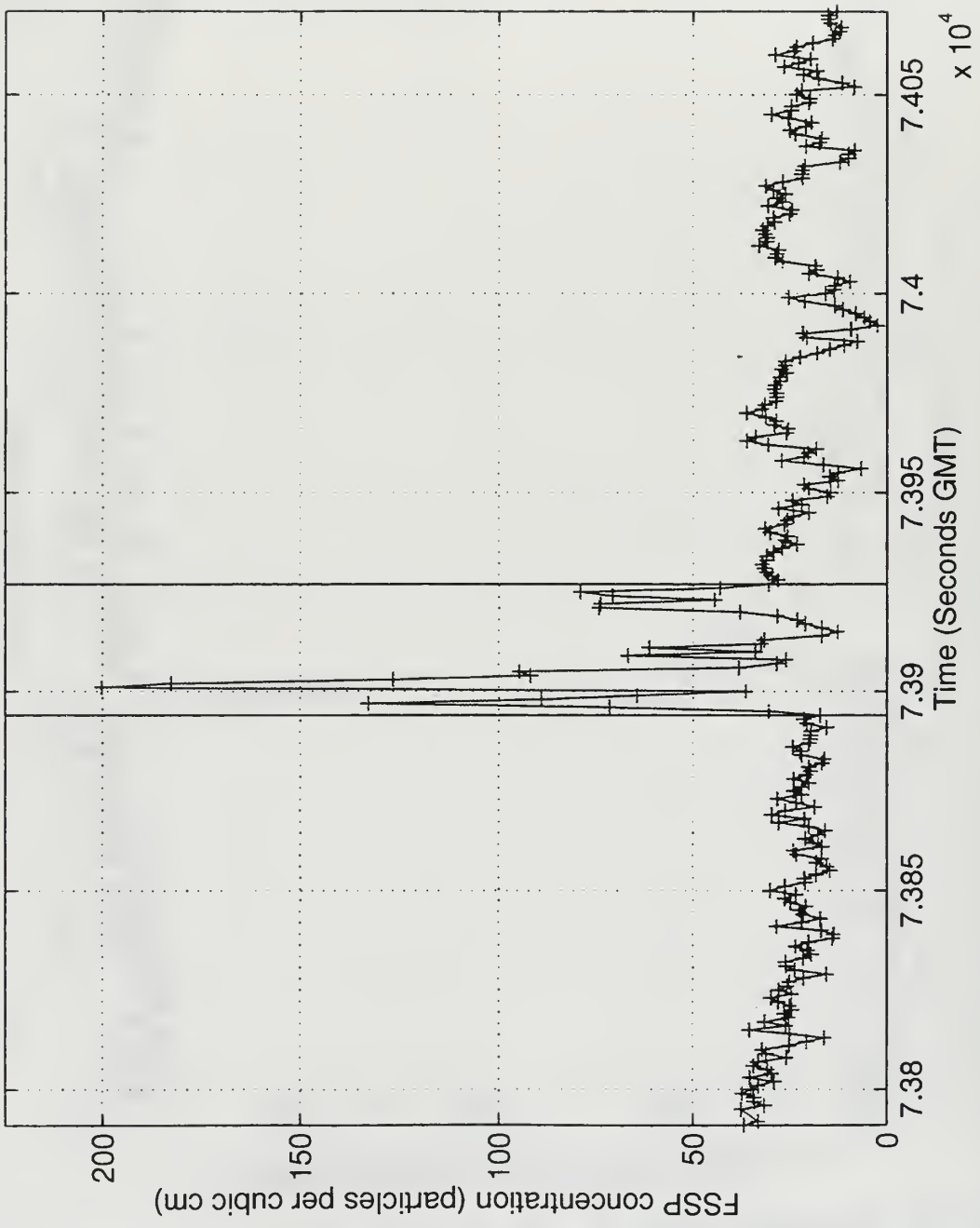

Figure B6 Cross-track plots of the FSSP detected droplet concentration measurements for flight A338, start time 20:29:51.

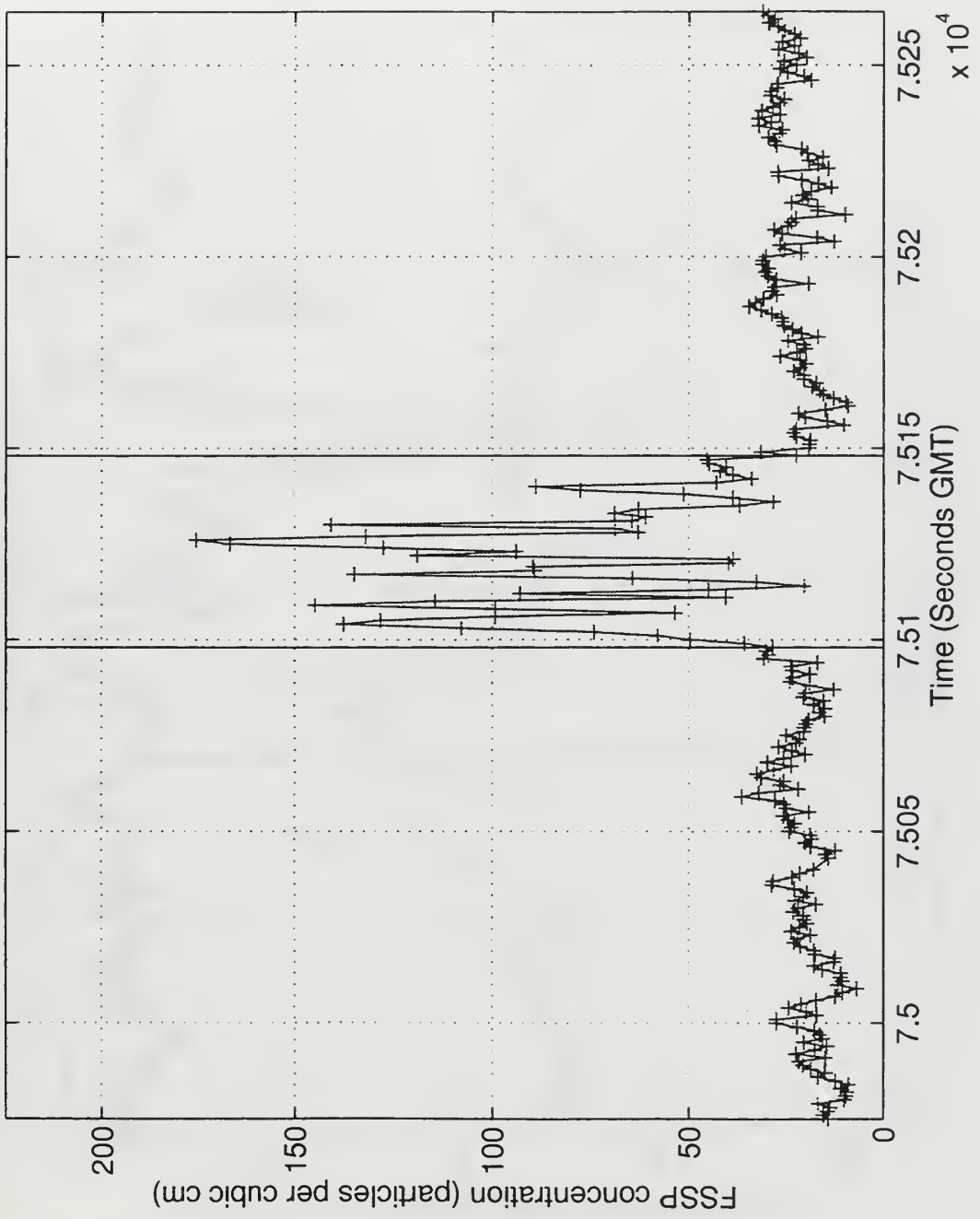

Figure B7 Cross-track plots of the FSSP detected droplet concentration measurements for flight A338, start time 20:49:35.

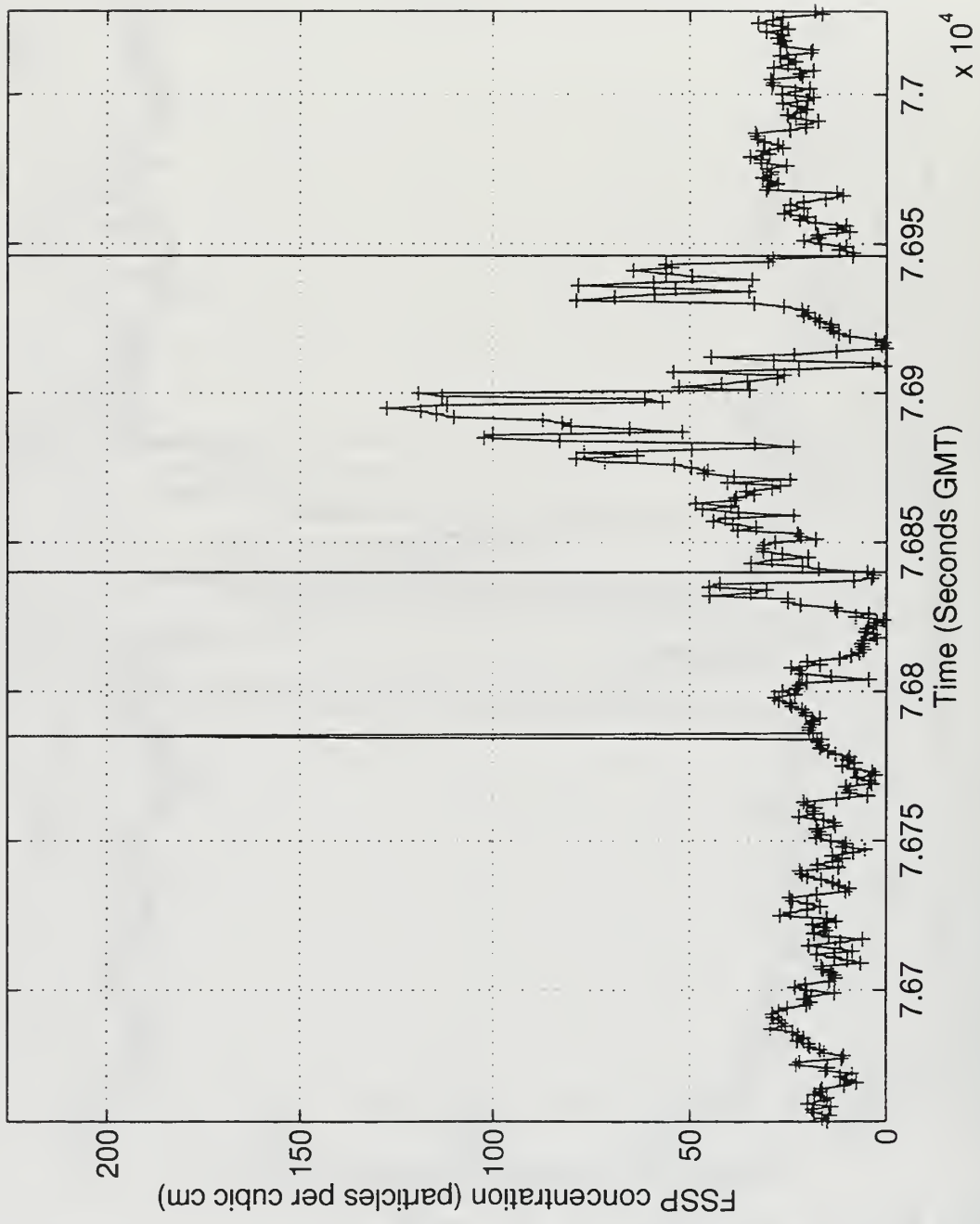

Figure B8 Cross-track plots of the FSSP detected droplet concentration measurements for flight A338, start time 21:17:36.

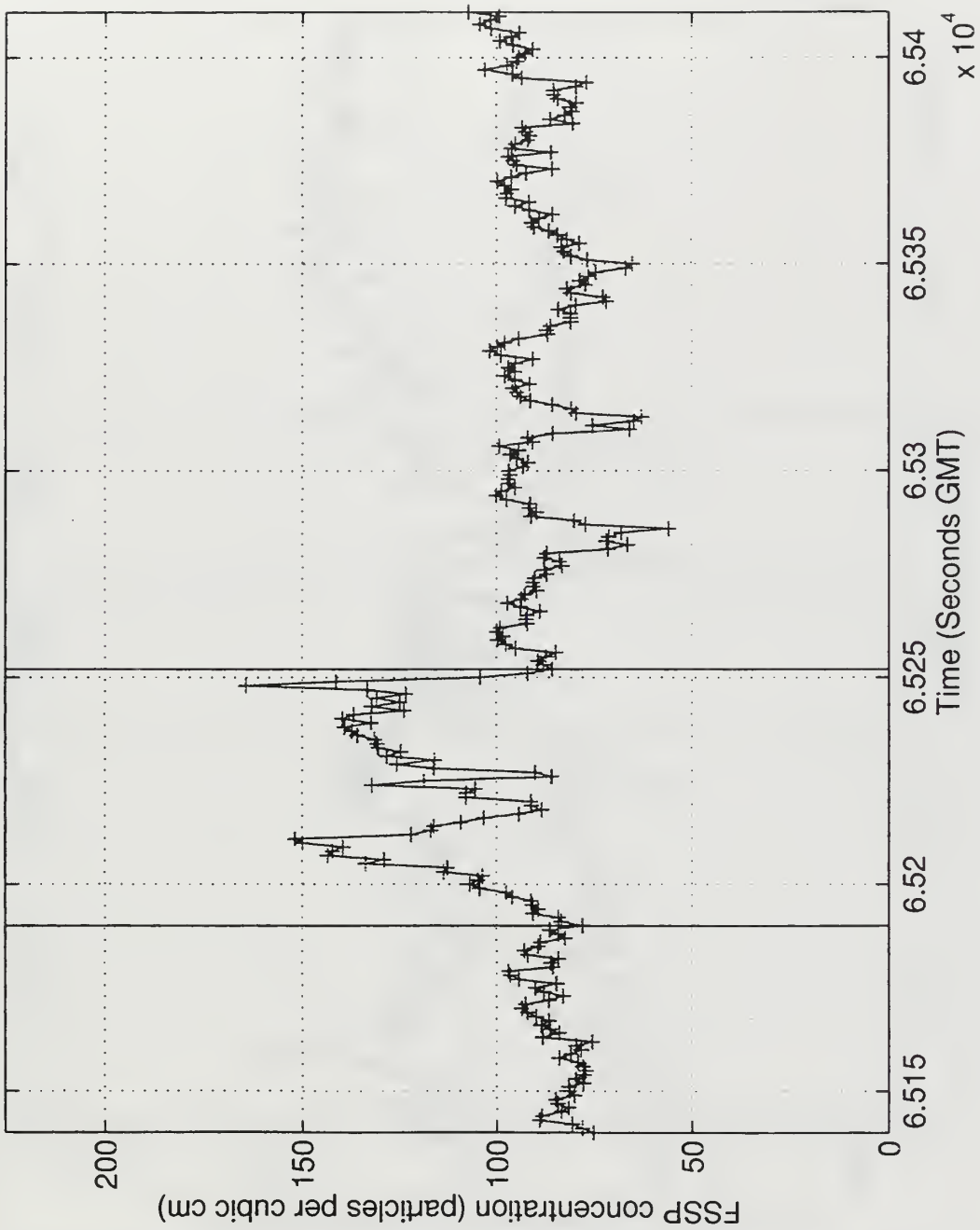

Figure B9 Cross-track plots of the FSSP detected droplet concentration measurements for flight A346, start time 18:05:40.

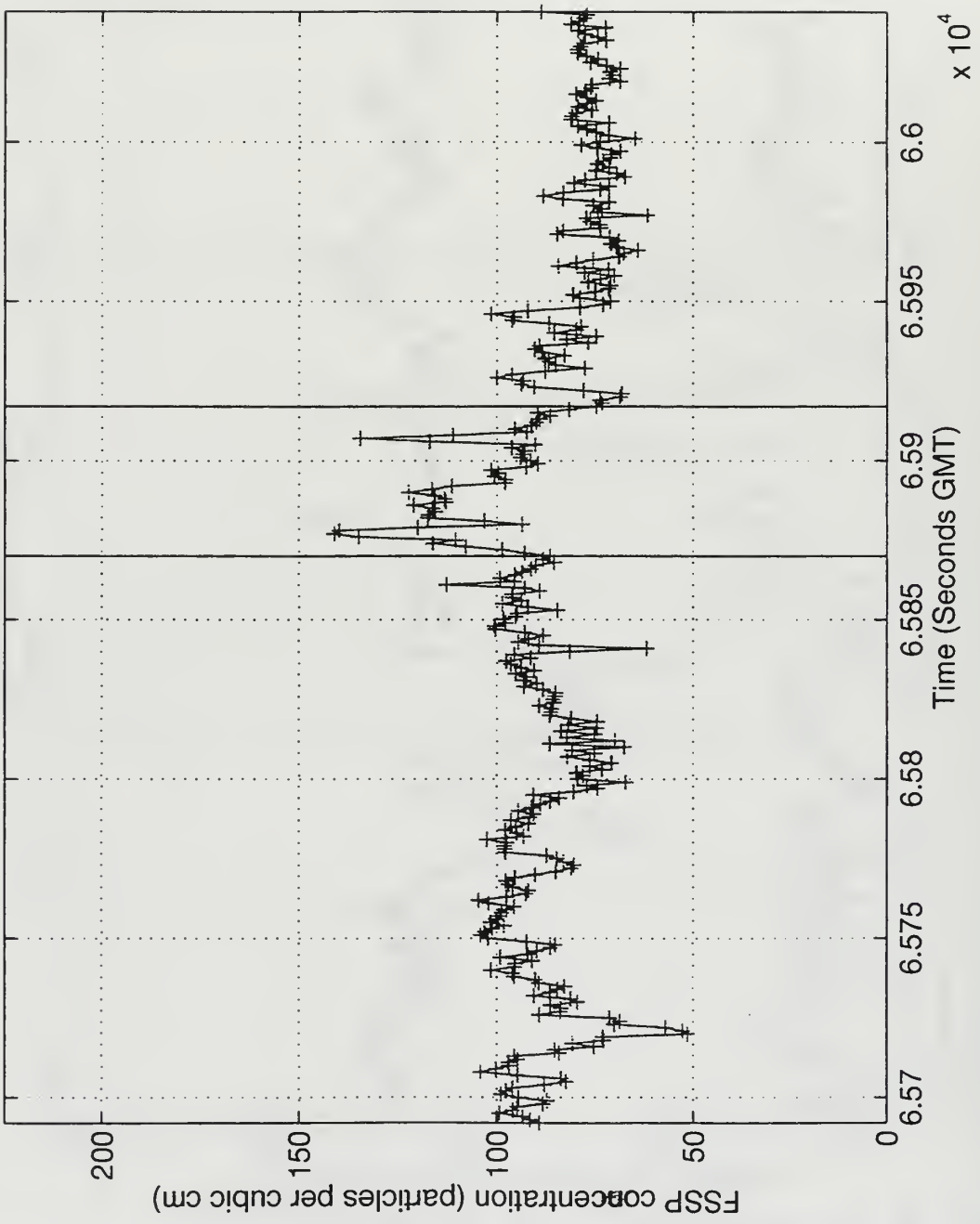

Figure B10 Cross-track plots of the FSSP detected droplet concentration measurements for flight A346, start time 18:14:52.

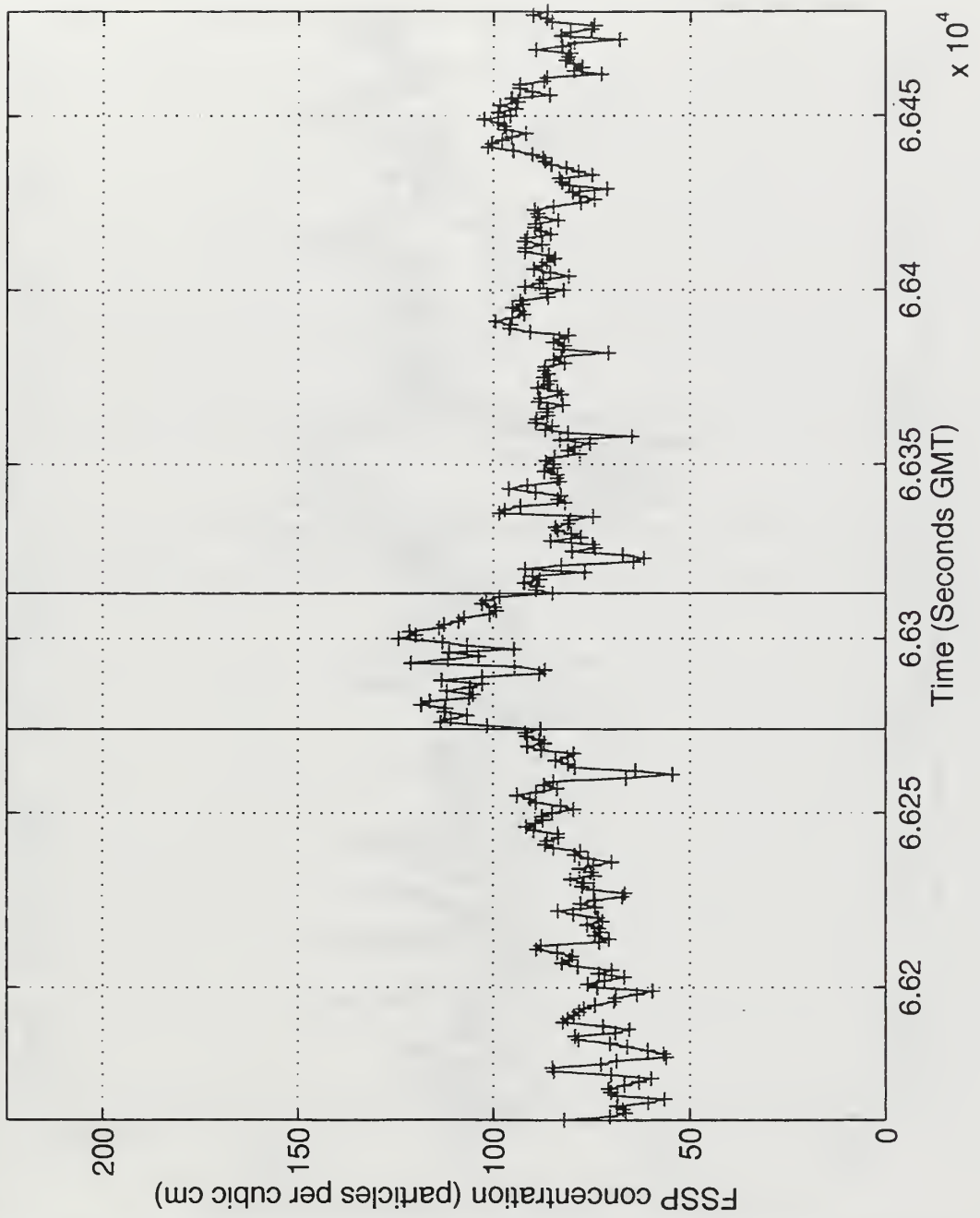

Figure B11 Cross-track plots of the FSSP detected droplet concentration measurements for flight A346, start time 18:22:42.

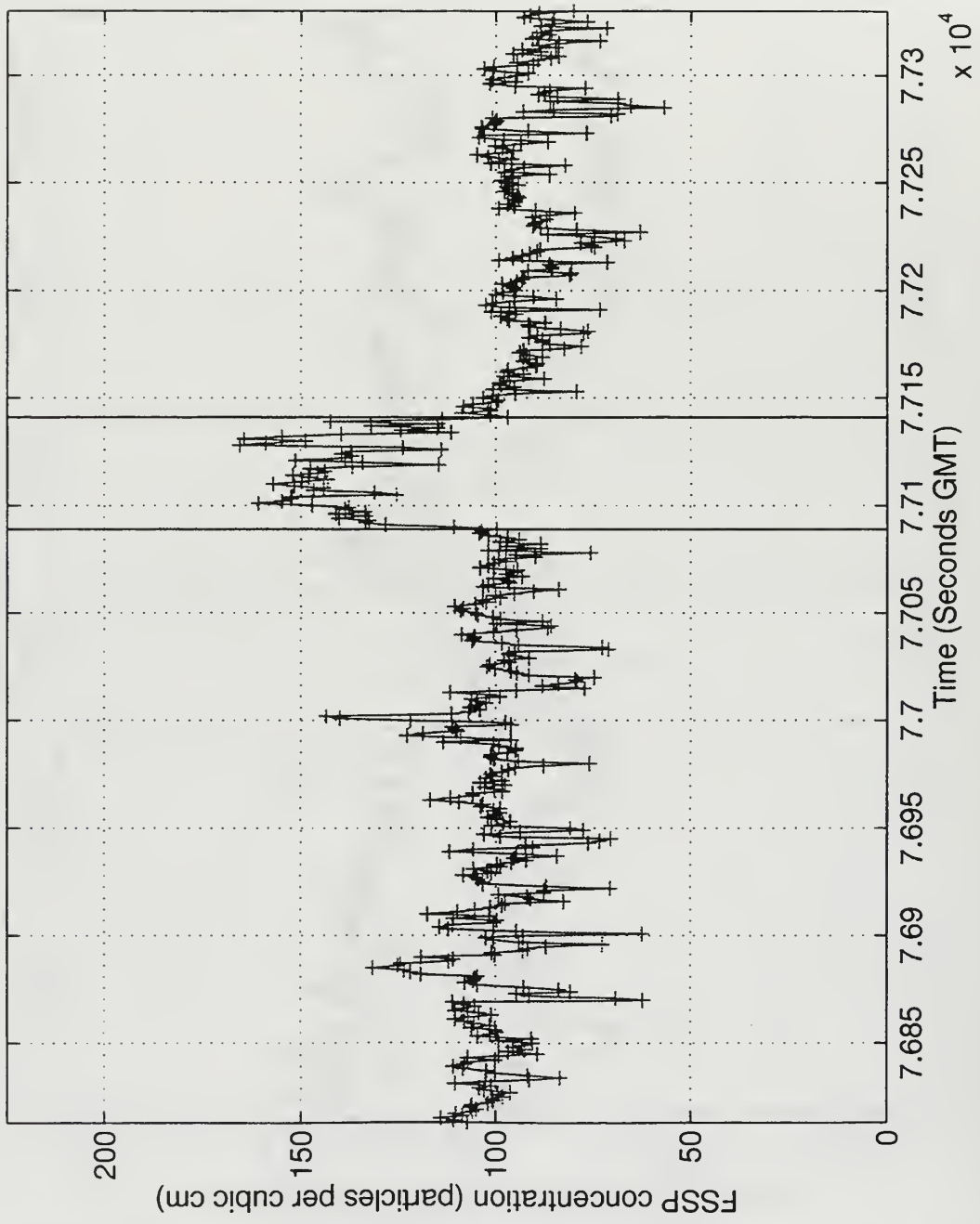

Figure B12 Cross-track plots of the FSSP detected droplet concentration measurements for flight A346, start time 21:20:13.

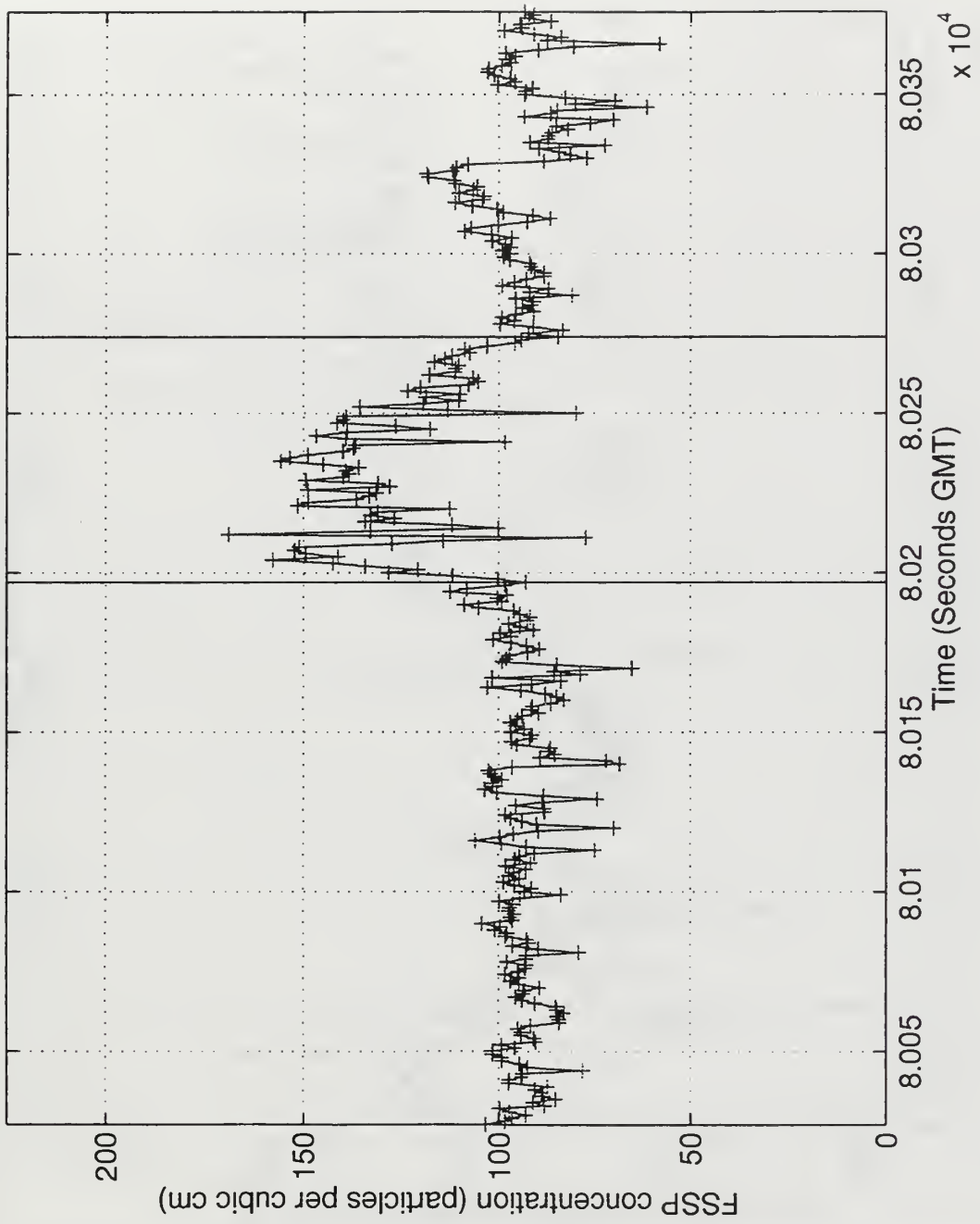

Figure B13 Cross-track plots of the FSSP detected droplet concentration measurements for flight A346, start time 22:13:47.

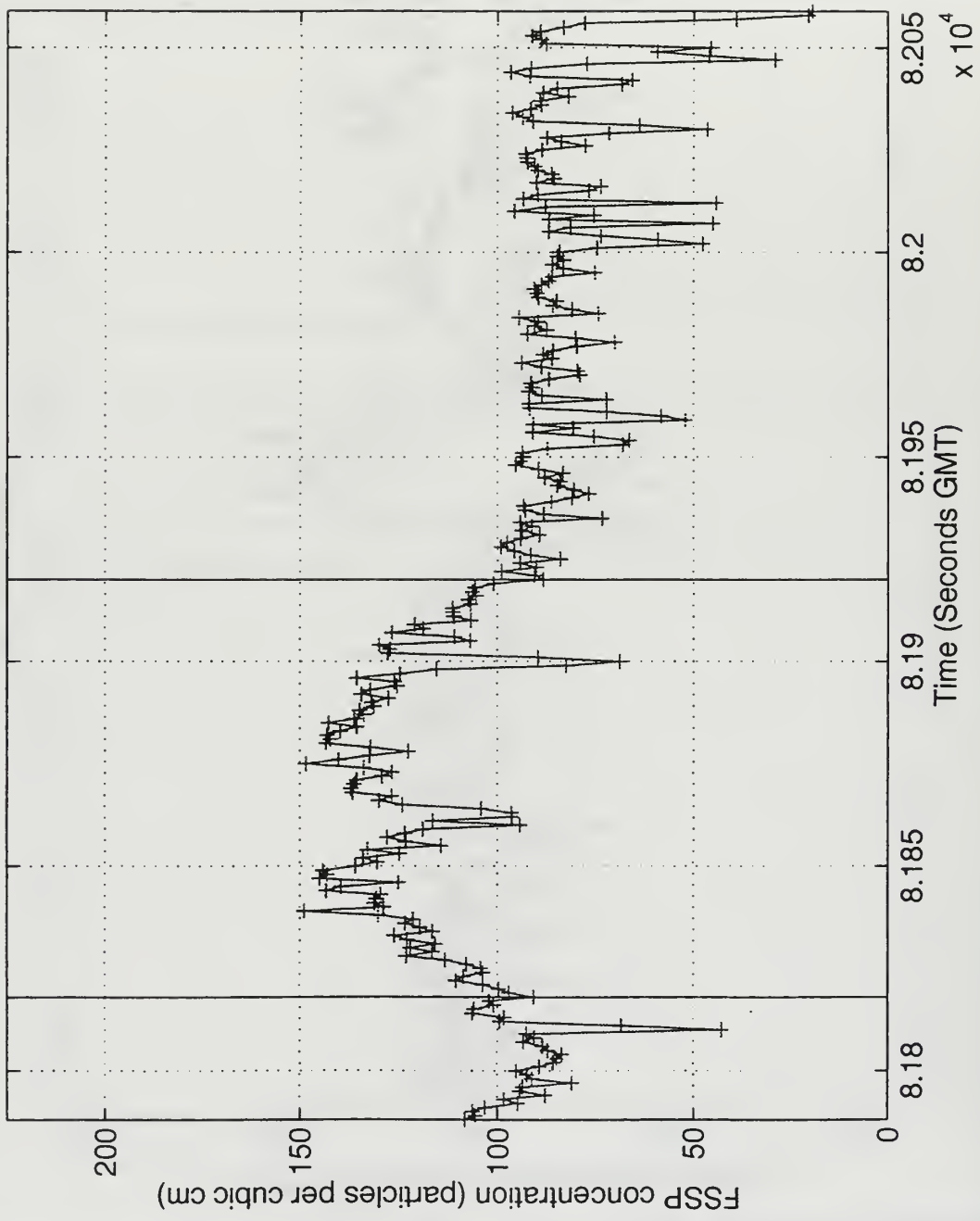

Figure B14 Cross-track plots of the FSSP detected droplet concentration measurements for flight A346, start time 22:43:08.

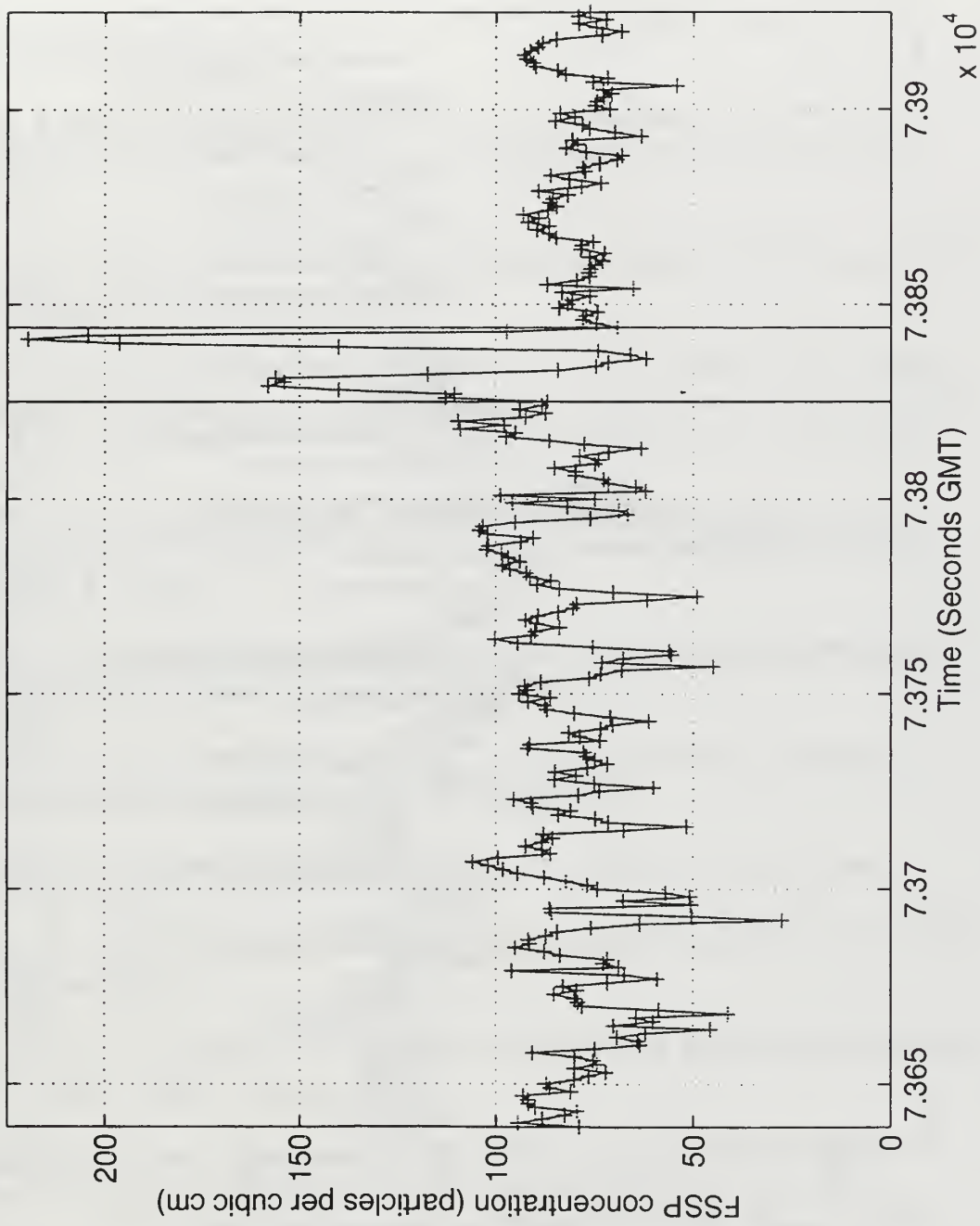

Figure B15 Cross-track plots of the FSSP detected droplet concentration measurements for flight A347, start time 20:27:19.

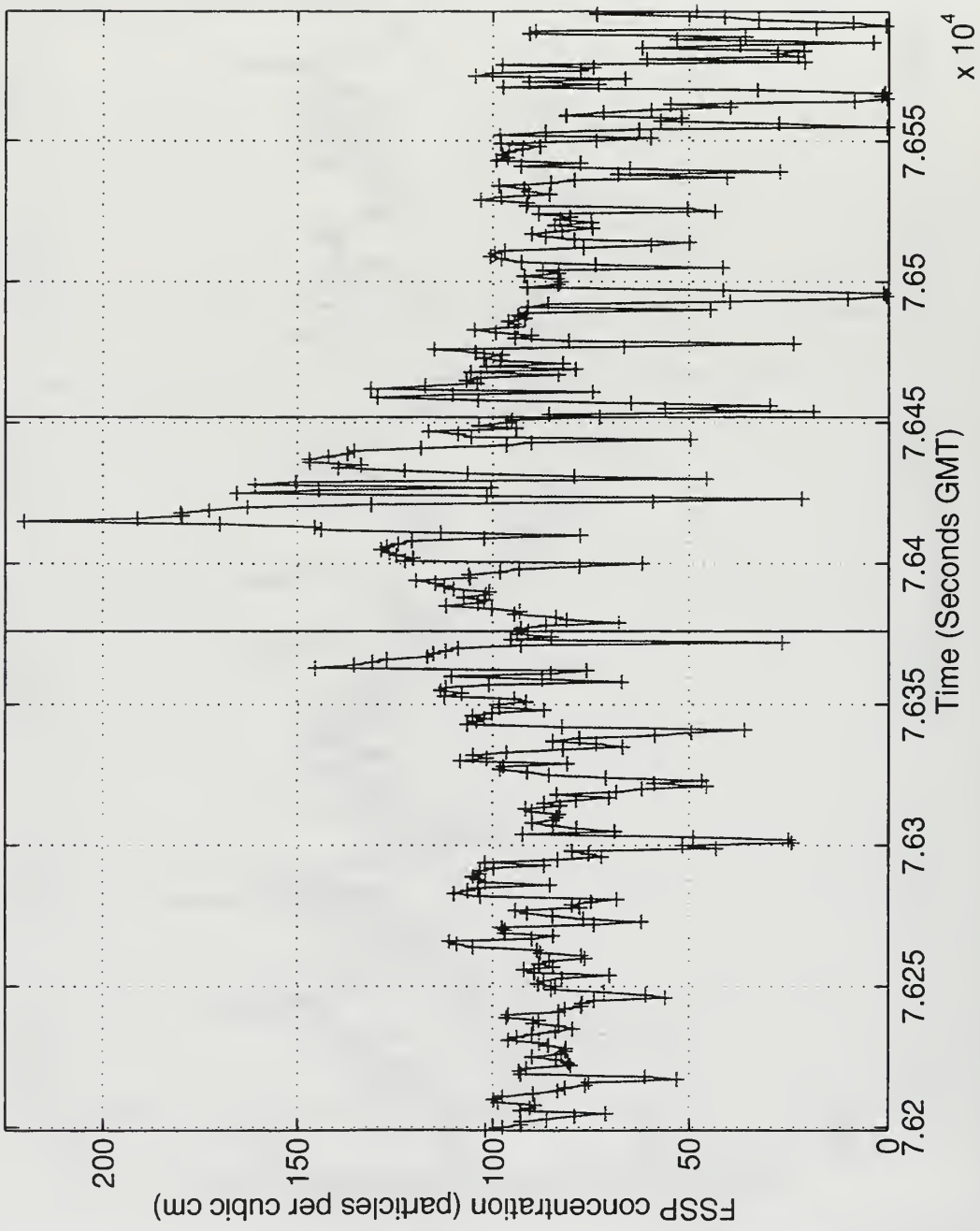

Figure B16 Cross-track plots of the FSSP detected droplet concentration measurements for flight A347, start time 21:09:59.

LIST OF REFERENCES

Albrecht, B.A., 1989: Aerosols, cloud microphysics and fractional cloudiness. *Science*, 245, 1227-1230.

Brenner, J., 1994: Continental aerosol effects on stratocumulus microphysics during MAST 1994. M.S. Thesis, Naval Postgraduate School, Monterey, CA, 60pp.

Brown, A. , 1994: Temporal effects of ship tracks on clouds. M.S. Thesis, Naval Postgraduate School, Monterey, CA, 60pp.

Charlson, R.J., J.E. Lovelock, M.O. Andreae, and S.G. Warren, 1987: Oceanic phytoplankton, atmospheric sulfur, cloud albino, and climate. *Nature*, 326, 655-661.

Charlson, R.J., S.E. Schwartz, J.M. Hales, R.D. Cess, J.A. Coakley Jr., J.E. Hansen and D.J. Hofman, 1992: Climate forcing by anthropogenic aerosols. *Science*, 255, 423- 430.

Chartier, R. E., 1995: Composite Ship track Characterizations. M.S. Thesis, Naval Postgraduate School, Monterey, CA, 76pp.

Coakley, J.A. Jr., R.L. Bernstein and P.A. Durkee, 1987: Effect of ship-stack effluents on cloud reflectivity. *Science*, 237, 1020-1022.

Conover, J.H., 1966: Anomalous Cloud Lines. *J. Atmos. Sci.*, 23, 778-785.

Durkee, P.A., 1994: Monterey Area Ship track Experiment [CNO Project K-1420] Science Plan. 42pp.

Gibbs, M., D.W. Johnson, D. Percival, and J. Taylor 1994: MAST Flight Summary for U.K. C-130. 131pp.

Hindman, E.E., 1990: Understanding ship-trail clouds. Preprints of 1990 Conference on Cloud Physics, 23-27 July, 1990, San Francisco, CA, A.M.S., Boston, MA. IPCC (The Intergovernmental Panel on Climate Change), 1994: Radiative Forcing of Climate, World Meteorological Organization and United Nations Environmental Program, in press.

King, M.D.,L.F. Radke, and P.V. Hobbs 1993: Optical Properties of Marine Stratocumulus Clouds Modified by Ships. *J. Geophys. Res.*,98, 2729-2739.

Mineart, G.M., 1988: Multispectral satellite analysis of marine stratocumulus cloud microphysics. M.S. Thesis, Naval Postgraduate School, Monterey, CA, 138pp.

Nielson, K.E., and P.A. Durkee, 1992: A robust algorithm for locating ship track cloud features using 3.7 micron satellite data. Preprints to the Papers on the 6th Conference on Satellite Meteorology and Oceanography, 5-10 January, 1992, Atlanta, GA.

Nielson, K.E., 1996: Personal communications.

Noonkester, V.R., 1984: Droplet Spectra Observed in Marine Stratus Cloud Layers. *J. Atmos. Sci.*, 41, 829-845.

Percival, D., 1995: A Guide to the Data from the Meteorological Research Flight held within the M.A.S.T. Data Archive. 46pp.

Platnick, S., S. Twomey, 1994: Determining the Susceptibilty of Cloud Albino to Changes in Droplet Concentration with the Advanced Very High Resolution Radiometer. *J. Appl. Meteor.*, 33, 334-347.

Porch, W.M., C.J. Kao, and R.G. Kelley, 1990: Ship trails and ship induced cloud dynamics. *Atmos. Environ.*, 24A, 1051-1059.

Radke, L.F., J.A. Coakley, Jr. and M.D. King, 1989: Direct and remote sensing observations of the effects of ships on clouds. *Science*, 246, 1146-1149.

Rogerson, S.D., 1995: Implications of Ship tracks on Ship Surveillance. M.S. Thesis, Naval Postgraduate School, Monterey, CA, 57pp.

Skupniewicz, C.E., 1995: Personal communications.

Siquig, R.A., 1991: A Simple Cloud Reflectance Model for Ship Tracks in Clouds. Naval Oceanographic and Atmospheric Research Laboratory, Technical Note 175., Monterey, CA, 38pp.

Stephens, G.L., 1994: Remote Sensing of the Lower Atmosphere, An Introduction. Oxford University Press, Inc., New York, NY.

Trehubenko, E.J., 1994: Ship tracks in the Californian Stratus Region: Dependency on Marine Atmospheric Boundary Layer Depth. M.S. thesis, Naval Postgraduate School, Monterey.

INITIAL DISTRIBUATION LIST

	N. Copies
1. Defense Technical Information Center 8752 John J. Kingman Rd., STE 0944 Ft. Belvoir, Virginia 22060-6218	2
2. Dudley Knox Library Naval Postgraduate School 411 Dyer Rd. Monterey, California 93943-5101	2
3. Chairman (Code MR/Hy) Department of Meteorology Naval Postgraduate School Monterey, California 93943-5002	1
4. Chairman (Code OC/Bf) Department of Oceanography Naval Postgraduate School Monterey, California 93943-5002	1
5. Professor Philip Durkee (Code MR/De) Department of Meteorology Naval Postgraduate School Monterey, California 93943-5002	1
6. Professor Kenneth Davidson (Code MR/Ds) Department of Meteorology Naval Postgraduate School Monterey, California 93943-5002	1
7. Mr. Bob Bluth Office of Naval Research Code 4513 Room 522 800 North Quincy Street Arlington, Virginia 22217-5000	1

8. Mr. David Johnson — 1
Office of Naval Research
Code 4513 Room 522
800 North Quincy Street
Arlington, Virginia 22217-5000

9. Oceanographer of the Navy — 1
Naval Observatory
34th and Massachusetts Avenue NW
Washington, DC 20390-5000

10. Commander — 1
Naval Observatory
34th and Massachusetts Avenue NW
Washington, DC 20390-5000

11. Chief of Naval Research — 1
800 North Quincy Street
Arlington, Virginia 22217-5000

12. Commanding Officer — 1
Fleet Numerical Meteorology and Oceanography Center
Monterey, California 93943

13. LT Raymond Chartier Jr. — 1
MEMOC-Rota
PSC 819, Box 31
FPO AE 09645-3200

14. LCDR Scott A. Tessmer — 2
237 Tunisia Road
Seaside, California 93955